

Passive Bipedal Running

Tad McGeer

CSS-IS TR 89-02

PASSIVE BIPEDAL RUNNING

Tad McGeer*

Simon Fraser University
Burnaby, British Columbia, Canada V5A 1S6

11 April 1989

Abstract

Human-like running is a natural dynamic mode of a simple mechanical biped. Such a machine consists of two telescoping legs with linear springs, connected by a hip joint with a torsional spring. It will run passively; *i.e.* no pattern of forcing is required to generate the gait. With careful design its energy consumption can approach zero, but in any case the passive cycle can be "pumped" by various means to sustain running over a range of speeds and slopes. Passive running can also be realised over a wide range of mechanical design parameters. Some parameter sets produce cycles which are inherently stable; otherwise the mode can be actively stabilised by a simple control law. Thus the passive running model offers an effective foundation for design of practical running machines, and also provides insight into the physics of human locomotion.

*School of Engineering Science. (TMCG@SFU.MAILNET, Tad_McGeer@cc.sfu.ca)

Contents

1	Passive dynamics in bipedal locomotion	1
2	The model	2
3	The cycle	2
4	The mathematics	3
5	Speed control	6
6	Stability	8
7	Running energetics	10
7.1	Aerodynamic drag	10
7.2	Landing impulses	11
7.3	Joint friction	12
7.4	Total specific resistance	13
8	“Active” energy supply	13
8.1	Stance/torso torque	14
8.2	Stance thrust	14
9	Active stabilisation and foot placement	16
10	Large perturbations	17
11	Finite friction	18
12	Summary of parametric effects	20
12.1	Foot radius	20
12.2	Leg inertia	22
12.3	Leg mass centre	22
12.4	Hip mass	22
13	Conclusion	23
A	General equations of motion	24
B	Flight phase	26
C	Stance phase while not slipping	27
D	Stance phase while slipping	28

<u>Passive bipedal running</u>	iii
E Phase transition conditions	29
E.1 Numerical search for the switching points	29
F Landing impulse	30

Roman

A_f	frontal area
c	nominal foot→leg CM distance (fig. 1)
c_T	hip→torso CM distance (14)
C_D	aerodynamic drag coefficient (8)
d	viscous damping coefficient (31), (57)
E	energy
F	force
F_\perp	force normal to the stance leg axis (fig. 17)
g	gravitational acceleration (fig. 1)
H	angular momentum (42)
I	moment of inertia (54), (55), (75), (76), (77), (78), (79)
K	spring constant (fig. 1)
l	leg length (fig. 1)
l_O	nominal leg length (fig. 1)
l_{zf}	leg length for zero spring force (16)
l_θ	stance thrust coefficient (16)
m	mass (fig. 1)
R	foot radius (fig. 1)
$\vec{r}_{CM/C}$	biped CM → stance leg CM vector (44)
\vec{r}_{HC}	hip → stance leg CM vector (59)
$\vec{r}_{H/CM}$	hip → biped CM vector (45)
\vec{r}_{HF}	hip → swing leg CM vector (60)
$\vec{r}_{O/CM}$	origin → biped CM vector (66)
\vec{r}_{PH}	contact point → hip vector (61)
r_{gyr}	radius of gyration
\tilde{S}	stride function (1)
$\nabla \tilde{S}$	gradient of \tilde{S} (2)
$\nabla_c \tilde{S}$	partial of \tilde{S} w.r.t. l_θ, T_T
s	take-off → take-off translation
SR	specific resistance (7)
T	torque
T_T	stance/torso torque (13)
V	linear velocity
v_{foot}	foot slip rate
v_O	bounce parameter (37)
w	leg axis → mass centre offset (fig. 1)
\hat{x}_C	unit vector along the stance leg (68)

Greek

\hat{y}_C	unit vector normal to the stance leg
z	eigenvalue of the S-to-S equations (6)
γ	slope, positive downhill (fig. 1)
γ_P	slope for passive running
$\Delta\theta$	change from steady-cycle θ (6)
$\Delta\Omega$	change from steady-cycle Ω (6)
ΔE	energy change
Δl_{CT}	change from steady-cycle l_{CT} (6)
Δl_{eq}	change in static equilibrium from l_O (35)
ζ	damping ratio (65)
θ	angle relative to surface normal (fig. 1)
μ	friction coefficient
ρ	air density
τ	dimensionless time $\sqrt{l_O/g}$
Ω	angular speed
ω_l	leg-compression frequency
ω'_l	leg-compression frequency modified by centrifugal effect (34)
ω_{sc}	scissor frequency

Sub- and superscripts

0	steady cycle conditions
C	stance leg
c	contact
CM	biped's mass centre
F	swing leg
g	due to gravity
n	step index
T	take-off, torso
x	normal to the ground (fig. 1)
y	along the ground (fig. 1)
$+$	immediately before landing 
$-$	immediately after landing 

1 Passive dynamics in bipedal locomotion

It is said that one should walk before one tries to run. Hence we begin discussion here with a brief review of studies in walking, from which our running analysis derives. It is commonly thought that walking is an *active* process, that is, some complex pattern of muscular activity is required to produce the motion. Actually, however, walking can be sustained *passively* by a simple interaction of gravity and inertia. We have built a machine which demonstrates the effect. It is actually little more than two rigid legs connected by a pin joint (*cf.* fig. 1). If left standing upright with legs together, the machine topples like a pencil on its point. (It can only topple longitudinally; sideways motion is prevented by building each leg as a pair of crutches connected by a rigid link.) However if placed on a shallow downhill slope (which provides a source of energy) and given appropriate initial conditions, it settles after a few steps into a steady gait quite comparable to human walking. Passive dynamic effects both generate and stabilise the gait; the only active intervention is for lifting of the swing feet to prevent toe-stubbing.

Passive walking provides a simple but rigorous model of human locomotion, as well as a foundation for design of practical bipedal machines. [McGeer 88] develops the theory for exploiting passive dynamics in a biped capable of climbing and descending shallow slopes ($\approx \pm 10\%$) and of using irregularly-spaced stepping stones. We expect to have such a biped ready for tests by the fall of 1989. We also plan future work on steep slopes and stairs, and on lateral balance and steering.

Over the last year we have also become interested in bipedal running. In part this is just a matter of curiosuty, but we also have a strong practical motivation: speed. As noted by [Alexander 77], bipedal walking is restricted to speeds somewhat less than \sqrt{gl} , where g is the gravitational acceleration, and l the leg length. Breaking the " \sqrt{gl} barrier" calls for a different type of gait, namely running. The reason is easily explained. [McMahon 78] has demonstrated that running and walking are distinguished most reliably by the height of the biped's mass centre at midstance. In walking midstance is the instant of *maximum* height, as the hip rotates over a rigidly extended stance leg. Centrifugal effect on this trajectory lightens the contact force at the foot; as the speed approaches \sqrt{gl} the force goes to zero. (You will feel this if you try to walk unusually fast.) In running, on the other hand, the leg compresses so that midstance is the instant of *minimum* height. Compression diminishes centrifugal effect, so the leg remains in contact through midstance. Normally the subsequent extention is sufficiently vigorous to cause lift-off, which produces a *flight phase* after each stance period. ([McMahon 84] has shown that it can disappear under unusual circumstances, but here we will treat only cycles which include the flight phase.)

In view of the appeal of passive dynamic walking, we naturally wondered whether there might be such a thing as passive dynamic running. Upon investigation we found that indeed there is. That is, we now have an analytical model which runs passively, and since it is similar to that proved experimentally for walking we expect that it can be realised in practice. Here we present the model, and use it both to explain some features of human running and to suggest techniques for design and control of running machines.

2 The model

Our analysis is developed for a two-dimensional biped as shown in figure 1. It has semicircular feet, straight legs, and a point mass at the hip which represents the torso. ([McGeer 88] has shown that addition of an extended torso has a relatively small effect.) In the "walking" version of this model the stance leg is kept rigid. As it rocks forward, the free leg swings ahead in a pendulum action, and lands with an impact which we treat as inelastic and impulsive. This transfers support instantaneously, so a new stance phase starts immediately where the old one left off. The impulsive impact dissipates some energy, which is recovered by descending a shallow slope.

In the running model we must arrange for stance compression, so we introduce a spring parallel to each leg's axis. This allows the whole assembly to bounce between stance and flight phases, as suggested by [Raibert 86]. Note that a spring cannot transmit an impulse parallel to its axis. Therefore foot-strike conditions are quite different in the running and walking models. In walking the landing impulse is usually almost parallel to the leg axis; in running any impulse must be *normal* to the axis. Often there is no impulse at all.

One more spring, acting in torsion, must be introduced at the hip in order to recover the swing leg. In walking the pendulum effect alone is sufficient for this purpose, but in running the stance time is much shorter, and moreover the pendulum effect is much reduced. Since the stance leg is now a spring, substantial "hanging" force at the hip does not develop until well after foot strike. In the meantime a freely-hinged swing leg would remain more or less in free fall, and so wouldn't get the torque necessary for recovery. The hip spring takes over this job, through the action of a "scissor mode". Scissoring is most easily visualised by imagining the model free in space, with the legs oscillating back and forth at the characteristic inertia/spring frequency. Stance/flight bouncing during locomotion has a remarkably small effect on this scissor motion, as we will demonstrate presently. Of course one proviso is that the swing leg must be shortened during the stance phase in order to keep its foot clear of the ground. We presume that this doesn't change the leg's inertia. By the same token, all of the mass in our model is taken to be *above* the legs' axial springs.

All of our analysis is done in dimensionless terms, with total mass m , relaxed leg length l_0 and gravity g providing the base units. (Readers not familiar with such a formulation need only note that one unit of time is therefore $\sqrt{l_0/g}$, one unit of inertia ml_0^2 , one unit of stance spring stiffness mg/l_0 , etc.)

3 The cycle

Exact cycle calculations involve several coupled nonlinear differential equations with a formidable number of terms. The volume of mathematics might suggest complexity, but the physics is really quite simple. In essence running is just a scissor-mode oscillation proceeding in phase with vertical bouncing. An example will illustrate. Figure 2 shows a cycle with parameters chosen, for the sake of interest, to match the stride length and flight/stance times in a set of human data measured by [McMahon 87]. (Parametric variations are discussed later in the paper.)

[Raibert 86] has made extensive observations on symmetry in running, and so it is especially interesting that symmetry is inherent in the passive model. That is, if you were shown a film of the cycle in figure 2 you couldn't tell whether it was running forward in time and left-to-right in space, or backward in time and right-to-left in space. (This is true despite the timing offset between peak angles during the flight phase; that is just a consequence of rigid-body rotation superimposed upon the scissor mode.) A remarkable consequence of symmetry is *conservation of energy*. Since in this example the feet are massless, the springs undamped, and the air resistance zero, the only mechanism for energy dissipation would be an impulse at foot strike (which, as explained earlier, would have to be normal to the leg axis). But in a symmetric run foot strike is the mirror image of take-off; since no impulse occurs at take-off, none can occur on landing. Unfortunately this happy situation arises only if the model parameters introduce no bias or irreversibility. If instead there is an offset between the leg axes and mass centres, or friction, then the cycle becomes asymmetric and a source of energy (such as a downhill slope) is needed to keep it going (figures 10, 11).

Now observe the timescale. In this example the scissor-mode period is about $2.57\sqrt{l_0/g}$ (64). By comparison, two cycles of figure 2 (*i.e.* one full back-and-forth cycle for each leg) would take $2.52\sqrt{l_0/g}$. Thus the scissor frequency is almost equal to *cadence*, which is normally defined as the frequency of full strides. This result applies not only in the example at hand, but also over a wide range of speeds, step lengths, and other model parameters. The implication is that bouncing has little effect on the scissor mode.

Thus knowing only the inertial properties of the model, and without elaborate calculation, one can predict cadence with high accuracy. (This is equally true of walking, for which the swing leg's pendulum frequency is the key parameter [McGeer 89].) One might ask if other features of the cycle can be so easily understood, for example not only the total time for a stride, but also the ratio of stance and flight times. Here the appropriate conceptual model is vertical bouncing. Thus one can imagine a mass bouncing *straight up-and-down* on the stance spring, with period and stance/flight ratio determined by the total energy and mass/spring frequency. Such models have been analysed by [McMahon 87] and [Bühler 88]. However, while the scissor mode is not much affected by bouncing, it turns out that bouncing is strongly affected by the scissor motion. Hence for accurate calculation of the stance/flight ratio one must use the full mathematical model.

Before we proceed it is worth noting that the phenomenon of bounce- and scissor-modes together generating locomotion applies beyond our own bipedal model. In work to be published, Marc Raibert has shown passive running of a monopod, in which the scissor mode acts between leg and torso. Again the scissor frequency predicts the cadence, but there is a difference in that the monopod takes only one step per scissor cycle rather than two.

4 The mathematics

In this section we will outline the method for running analysis, while leaving mathematical details – including the equations of motion – for the appendix (table 6). Consider a convenient reference point in the stride. We use take-off. At this point the following 6 state variables can

be specified independently:

1. stance and swing leg angles θ_{CT}, θ_{FT}
2. angular rates Ω_{CT}, Ω_{FT}
3. stance extention rate i_{CT}
4. sliding speed along the ground v_{footT} (zero if sliding is disallowed)

Note that angles are measured from the surface normal, *not* the vertical. These variables, combined with the condition that take-off occurs when the stance force vanishes, determine the leg length, and geometry then determines the position and velocity of the mass centre.

These various initial conditions are put into the free-fall equations, which are integrated forward until the opposite foot hits the ground. Usually it is a good approximation to specify that the impact stops the foot instantaneously, via an impulse normal to the leg axis. The impulse changes Ω_{CT} , Ω_{FT} , and i_{CT} (appendix F). These new initial conditions are put into the stance equations, and integrated forward until force vanishing indicates the next take-off. If the new take-off state is identical to the original, then the cycle is repetitive. We want to find such "re-entrant" conditions.

In some cases we use a variation on this scheme, with a different treatment of landing. Under certain circumstances which we will discuss, the impulsive-landing approximation gives physically implausible results. This situation is remedied by recognising that there is finite friction at the point of contact. Contact impulses are then precluded, and instead the foot may slide for some time after landing. In fact during stance there may occur several switches between forward-slipping, backward-slipping, and no-slipping boundary conditions; thus the stance integration must be done with some care.

In any case, whether the contact-force model uses zero-slip or finite-friction boundary conditions, we can think in terms of a *stride function* \vec{S} mapping take-off conditions from step n to step $n+1$:

$$\begin{bmatrix} \theta_{CT} \\ \theta_{FT} \\ \Omega_{CT} \\ \Omega_{FT} \\ i_{CT} \\ v_{footT} \end{bmatrix}_{n+1} = \vec{S} \begin{bmatrix} \theta_{CT} \\ \theta_{FT} \\ \Omega_{CT} \\ \Omega_{FT} \\ i_{CT} \\ v_{footT} \end{bmatrix}_n \quad (1)$$

We want to find an argument which maps onto itself. As a formal matter one should ask first whether solutions exist and are unique. Existence is by no means guaranteed; we will show cases where passive cycles are apparently impossible. However, existence seems to be the rule rather than the exception, and when solutions exist, they are *not* unique. In fact solutions such as in figure 2 are not even well-spaced; since the cycle is conservative, it can be sustained with *any* level of total energy. (With more energy the motion would have larger amplitude and so higher speed.) Hence to calculate an individual solution one must choose the energy level (plus all the parameters of the model). This is most conveniently done by specifying the take-off

stance angle θ_{CT} , which leaves only 4 (or 5 with friction) state variables to be found. If one knows *a priori* that a solution must be conservative, then this is the complete search space. Nonconservative cycles, however, require some nonzero slope to maintain energy balance, and in general this must be found simultaneously with the re-entrant state vector.

Thus the search space is 5-dimensional with zero slip, and 6-dimensional otherwise. Of course to describe \vec{S} as merely nonlinear over this space is to do injustice to its rather unfortunate complexities, so the search cannot be conducted analytically. Instead we resort to Newton's method, whereby an initial estimate for the solution is improved as follows. Define a gradient matrix

$$\nabla \vec{S} \equiv \left[\frac{\partial \vec{S}}{\partial \theta_{CT}} \quad \frac{\partial \vec{S}}{\partial \theta_{FT}} \quad \frac{\partial \vec{S}}{\partial \Omega_{CT}} \quad \frac{\partial \vec{S}}{\partial \Omega_{FT}} \quad \frac{\partial \vec{S}}{\partial i_{CT}} \quad \frac{\partial \vec{S}}{\partial v_{footT}} \right] \quad (2)$$

For small changes in the state variables and slope, the change in \vec{S} is approximated by the first-order terms of its Taylor series:

$$\vec{S} \left(\begin{bmatrix} \theta_{CT} \\ \theta_{FT} \\ \Omega_{CT} \\ \Omega_{FT} \\ i_{CT} \\ v_{footT} \end{bmatrix} + \begin{bmatrix} \Delta\theta_{CT} \\ \Delta\theta_{FT} \\ \Delta\Omega_{CT} \\ \Delta\Omega_{FT} \\ \Delta i_{CT} \\ \Delta v_{footT} \end{bmatrix} \right) \approx \vec{S} \left(\begin{bmatrix} \theta_{CT} \\ \theta_{FT} \\ \Omega_{CT} \\ \Omega_{FT} \\ i_{CT} \\ v_{footT} \end{bmatrix} \right) + \nabla \vec{S} \begin{bmatrix} \Delta\theta_{CT} \\ \Delta\theta_{FT} \\ \Delta\Omega_{CT} \\ \Delta\Omega_{FT} \\ \Delta i_{CT} \\ \Delta v_{footT} \end{bmatrix} + \frac{\partial \vec{S}}{\partial \gamma} \Delta\gamma \quad (3)$$

Therefore to satisfy the steady-cycle condition, from (1),

$$\begin{bmatrix} \theta_{CT} \\ \theta_{FT} \\ \Omega_{CT} \\ \Omega_{FT} \\ i_{CT} \\ v_{footT} \end{bmatrix} + \begin{bmatrix} \Delta\theta_{CT} \\ \Delta\theta_{FT} \\ \Delta\Omega_{CT} \\ \Delta\Omega_{FT} \\ \Delta i_{CT} \\ \Delta v_{footT} \end{bmatrix} \approx \vec{S} \left(\begin{bmatrix} \theta_{CT} \\ \theta_{FT} \\ \Omega_{CT} \\ \Omega_{FT} \\ i_{CT} \\ v_{footT} \end{bmatrix} \right) + \nabla \vec{S} \begin{bmatrix} \Delta\theta_{CT} \\ \Delta\theta_{FT} \\ \Delta\Omega_{CT} \\ \Delta\Omega_{FT} \\ \Delta i_{CT} \\ \Delta v_{footT} \end{bmatrix} + \frac{\partial \vec{S}}{\partial \gamma} \Delta\gamma \quad (4)$$

As explained earlier we leave θ_{CT} constant in our solution procedure. Solving for the adjustments required in the remaining take-off variables and the slope leaves (in the finite-friction case)

$$\begin{bmatrix} \Delta\theta_{FT} \\ \Delta\Omega_{CT} \\ \Delta\Omega_{FT} \\ \Delta i_{CT} \\ \Delta v_{footT} \\ \Delta\gamma \end{bmatrix} \approx \left(\begin{bmatrix} \partial \vec{S} & \partial \vec{S} \\ \frac{\partial \vec{S}}{\partial \theta_{FT}} & \frac{\partial \vec{S}}{\partial \Omega_{CT}} & \frac{\partial \vec{S}}{\partial \Omega_{FT}} & \frac{\partial \vec{S}}{\partial i_{CT}} & \frac{\partial \vec{S}}{\partial v_{footT}} & \frac{\partial \vec{S}}{\partial \gamma} \end{bmatrix} - \begin{bmatrix} 000000 \\ 100000 \\ 010000 \\ 001000 \\ 000100 \\ 000010 \end{bmatrix} \right)^{-1} \times \begin{pmatrix} \theta_{CT} \\ \theta_{FT} \\ \Omega_{CT} \\ \Omega_{FT} \\ i_{CT} \\ v_{footT} \end{pmatrix} - \vec{S} \begin{pmatrix} \theta_{CT} \\ \theta_{FT} \\ \Omega_{CT} \\ \Omega_{FT} \\ i_{CT} \\ v_{footT} \end{pmatrix} \quad (5)$$

(If sliding is disallowed, then the row and column associated with v_{footT} can be deleted.)

To find a solution, one evaluates (5) iteratively until convergence. In our experience if the starting point is reasonable and a solution exists then this technique will find it (to 5 figures in each state variable) in less than 10 iterations. Note that each iteration involves 6 (or 7 with v_{footT}) evaluations of \vec{S} ; once for the nominal value, and 5 (or 6) times to get the gradients, which we find numerically. (5) calls for quite a bit of calculation!

For the initial estimate it is sufficient with most parameter sets to use $\theta_{FT} = \pi - \theta_{CT}$, $\Omega_{CT} = -\Omega_{FT} = V$ where V is the speed anticipated in the solution, $i_{CT} \approx 1$ and $\gamma = 0$. Of course convergence is accelerated by starting from a solution previously obtained for a similar parameter set. One can do better still by adjusting this solution according to a linearisation such as (5), using gradients with respect to the parameters being varied.

Another approach is simply to generate initial conditions at random. This is perhaps naive, but it is also unbiased, and so can reveal behaviour which might otherwise go unnoticed. Table 1 provides an illustration. The first solution in the table is just that for vertical bouncing on a steep hill. The next corresponds to normal running. Notice that, as in figure 2, $\omega_{sc}\tau_0 \approx \pi$. In the next two $\omega_{sc}\tau_0 \approx 3\pi$ and 5π respectively. In these cases the legs are going through one and two full scissor cycles during the flight phase, rather in the style of a long-jumper. The bounce is more energetic than in normal running, in order to provide sufficient flight time. Needless to say, in this paper we are interested only in the "half-scissor" running cycle.

5 Speed control

As we mentioned earlier, the objective of running is speed. Consider then, as a first application of the steady-cycle solution, how speed can be controlled. A look at the cycle of figure 2 indicates the options. Increasing speed essentially means increasing the slope of angle vs time during the stance phase. Thus one could increase the angle subtended during stance, as shown in figure 3. Alternatively one could reduce the stance time, either directly by adjusting K_{leg} (figure 4) or indirectly by adjusting cadence, via K_{hip} (figure 7). Incidentally figures 3 and 4 provide further illustration that cadence is determined almost exclusively by the scissor

Table 1: Newton's method solutions for passive running cycles over 40 trials with random initial estimates in the range

$$\begin{aligned} 0 < \theta_{CT} &< \pi/2 \\ \pi/2 < \theta_{FT} &< \pi \\ 0 < \Omega_{CT} &< 2 \\ -2 < \Omega_{FT} &< 0 \\ 0 < l_{CT} &< 2 \end{aligned}$$

Parameters:

$$\begin{array}{llll} R = 0 & r_{gyr} = 1/3 \\ c = 0.7 & w = 0 \\ K_{leg} = 20 & K_{hip} = 0.2 \\ m_T = 0.8 & \theta_{CT} = 0.45 \end{array}$$

Newton's method converged in 16/40 cases, as follows:				
cases	1/40	10/40	4/40	1/40
θ_{FT}	3.59	2.64	2.30	2.25
Ω_{CT}	0	1.65	0.98	0.73
Ω_{FT}	0	-1.22	-0.47	-0.41
l_{CT}	arbitrary	0.90	1.28	1.89
γ	-0.45	0	0	0
s	0	1.36	3.03	5.01
τ_0	arbitrary	0.74	2.16	3.49
$\omega_{sc}\tau_0$	arbitrary	3.30	9.6	15.6

frequency; while the stance/flight ratio varies, $\tau_0 \approx \pi/\omega_{sc}$ continues to hold across the whole spectrum of normal running speeds.

Figures 3, 4, and 7 present the options for speed control, but they don't show any preference among them. A robot designer would therefore be free to choose for convenience. Presumably varying spring stiffness would entail some mechanical complexity, so the θ_{CT} -method would appear to be superior for a machine. A human, on the other hand, makes only small changes in θ_{CT} and cadence with speed ([McMahon 87], [Margaria 76]). Hence the principal control must be K_{leg} . Figure 4 shows failure of this technique at low speed due to vanishing of the flight phase, but in the usual speed range it is quite effective. We presume that physiological constraints are at work in setting human preferences, although purely physical factors might be revealed by a more accurate mechanical model of human running, *i.e.* with knee joints. A related question is how humans adjust the effective stiffness of their legs. Variable stiffness

suggests a device more elaborate than passive elasticity of muscles and tendons, so there must be an associated metabolic cost.

6 Stability

One should perhaps be grateful that an activity so apparently complex as running turns out to be no more than a natural mode of a simple machine. However, one should also ask nature for something more: inherent stability. In practice a running machine will be continuously perturbed; thus an unstable cycle, even though generated passively, would have to be stabilised actively (§9).

To investigate stability, suppose that on stride n the take-off conditions are perturbed from the steady-cycle values by $\Delta\theta_{CTn}$, $\Delta\theta_{FTn}$, etc.. If the perturbations are small, then the conditions at take-off on stride $n + 1$ are accurately estimated by the linear approximation of \vec{S} (3):

$$\begin{bmatrix} \Delta\theta_{CT} \\ \Delta\theta_{FT} \\ \Delta\Omega_{CT} \\ \Delta\Omega_{FT} \\ \Delta\dot{l}_{CT} \\ \Delta v_{footT} \end{bmatrix}_{n+1} \approx \nabla \vec{S} \begin{bmatrix} \Delta\theta_{CT} \\ \Delta\theta_{FT} \\ \Delta\Omega_{CT} \\ \Delta\Omega_{FT} \\ \Delta\dot{l}_{CT} \\ \Delta v_{footT} \end{bmatrix}_n \quad (6)$$

This is just a linear difference equation in standard form. Solutions are proportional to z^n , where z is any eigenvalue of $\nabla \vec{S}$. Thus if all have magnitude less than unity, then small disturbances decay over subsequent steps. If not, then disturbances grow and eventually the biped stumbles.

For illustration return to the cycle of figure 2. Slipping is excluded in this example, so $\nabla \vec{S}$ is only 5×5 . The eigenvalues and eigenvectors are listed in table 2. There are three modes, which prove to be quite typical of passive running; we will show many more examples.

Table 2: Stride-to-stride stability of the cycle in figure 2

mode	speed	swing		totter	
		mag.	\pm phase	mag.	\pm phase
eigenvalue	1	0.22	\pm 1.62	1.65	\pm 2.42
θ_{CT}	0.13	0.03	\pm 0	0.08	\pm 0
θ_{FT}	-0.08	0.44	\pm 1.85	0.23	\pm -2.06
Ω_{CT}	0.42	0.07	\pm -2.47	0.13	\pm -1.07
Ω_{FT}	-0.72	0.89	\pm -1.44	0.95	\pm 0.55
\dot{l}_{CT}	0.53	0.08	\pm 0.41	0.14	\pm 1.59

The “speed” mode is associated with non-uniqueness of the running solution, as we discussed earlier. Thus if elements in the take-off state vector are perturbed in the ratios listed

in table 2, then the motion shifts to a new steady amplitude and speed. Thus this cycle is neutrally stable with respect to speed changes. On the other hand a *non-conservative* cycle has a unique steady amplitude, so its speed mode becomes a slow convergence (figure 9).

The next mode we call "swing" because of the large θ_{FT} and Ω_{FT} components. It is not of great concern since perturbations in this mode are damped rapidly.

Finally we have the "totter" mode. The name refers to an oscillation about the steady cycle, which as in this example typically has a period of 2-3 strides. Here the totter mode is *unstable*. Unfortunately this instability is also quite typical. For example, the totter mode remains unstable across the whole range of normal running speeds, regardless of whether K_{leg} or θ_{CT} is used as the speed control. The respective root loci are plotted in figures 5 and 6.

The totter mode thus becomes the central issue in running stability. We have devoted much effort to searching for parametric variations which improve its behaviour. Several parameters can be adjusted to some good effect (table 5) and one is especially powerful: cadence. Cadence is most easily adjusted via K_{hip} ; figure 7 shows two examples of its effect. As K_{hip} increases, the totter eigenvalues generally diminish until their magnitude reaches unity. Further increase in K_{hip} beyond this point changes only the phase of the totter eigenvalues, while leaving the magnitude nearly constant. Meanwhile the swing mode remains well-behaved, and the speed mode unperturbed. Moreover with high cadence stability is maintained across a wide speed range. Figure 8 demonstrates this point with a locus similar to that in figure 5 but using a substantially stiffer hip spring.

Close comparison of these various root loci is well worthwhile. The underlying adjustments to the model are physically quite different between the plots, yet the loci have similar features. In each one can follow the totter eigenvalues converging along a broad outer arc, splitting left and right for some distance along the negative real axis, reversing, and (with larger K_{hip}) colliding and arcing back into the complex plane near the rim of the unit circle. Meanwhile the swing eigenvalues follow a smaller arc tending generally from left to right on the complex plane, and the speed eigenvalue remains fixed at $z = 1$. These features appear again and again as one examines the effect of various parameters on stability. Thus we are always looking for S-to-S eigenvalues on the inner "totter arc".

Comparison of the loci shown so far indicate that a combination of sufficiently high speed and K_{hip} puts the totter eigenvalues where we want them, and so gives the totter mode near neutral stability for small perturbations. Moreover example calculations using the "exact" S-to-S equations (1) indicate that nonlinearities have no strong effect on stability one way or the other (*cf.* figure 15). The situation, then, might be considered marginally acceptable, and can be improved by means which we will discuss in a moment. First, however, it should be noted that the requisite hip stiffness is large. The examples of figure 7 call for K_{hip} of at least 0.2 for neutral stability. The corresponding scissor period is 1.41 in units of $\sqrt{l_O/g}$ (64); or about 0.4 sec with $l_O = 0.9m$. Therefore cadence would be 2.5 full strides per second, which is at the top end of the human data cited by [Margaria 76], and considerably faster than indicated by the data of [McMahon 87] for jogging.

Having moved the totter eigenvalues near the unit circle, consider now how they can be brought firmly inside and so made unequivocally stable. We thought that damping might be effective, so we introduced some dissipation into the stance spring. Figure 9 shows the

results. Here we measure dissipation by the damping ratio $\zeta = d_{leg}/\sqrt{4K_{leg}}$ which one would observe if the model were oscillating vertically on the stance spring. (Some may prefer to measure dissipation by the *quality*; $Q = 1/2\zeta$. Alternatively one might just note that $\zeta = 0.05$ corresponds to $\approx 50\%$ energy loss during each vertical oscillation.) The effect is as desired: damping moves the eigenvalues in generally the same direction as higher speed and K_{hip} , but also bends the inner “totter arc” inside the unit circle.

There is a price, of course, and trading efficiency for inherent stability may seem a poor bargain when the alternative of active stabilisation is available. However the next section explains that dissipation is hard to avoid in practice, so one might as well get something out of it! Benefits accrue not only in the totter mode. Since on a given slope a dissipative cycle has a unique steady amplitude, the speed mode also becomes absolutely stable.

7 Running energetics

Of course practical running requires some means of energy supply other than going downhill, not only to balance dissipation, but also for climbing. We will examine alternatives in the next section, but first we will make some estimates of the “fundamental” efficiency of running.

Vehicle efficiency is commonly measured by specific resistance:

$$SR \equiv \frac{\text{resistive force}}{\text{weight}} = \frac{\text{mechanical work done}}{\text{weight} \times \text{distance travelled}} \quad (7)$$

For a gravity-powered device such as a glider or passive biped, the specific resistance is equal (for $SR \ll 1$) to the steady descent angle. For example, our gravity-powered biped walker needs a slope of about 2.5% to sustain a gait comparable to human walking [McGeer 89]. The energy is dissipated by the impulse at heel strike. Our next machine is expected to have a specific resistance of only 1% in a similar gait; the improvement is due to addition of a torso, which raises the mass centre and so attenuates the impulse [McGeer 88].

For running, on the other hand, we have seen that the landing impulse and specific resistance can go to zero. The implication that running therefore might be much more efficient than walking must come as a great surprise to anyone who jogs. Of course this suggestion is too optimistic; dissipation is unavoidable. Loss mechanisms include not only landing impulses, but also aerodynamic drag and damping in the springs. One might also add foot slip to the list, but this causes negligible dissipation on surfaces with reasonable traction (figure 18). Also some energy must be used to clear the swing foot during stance, but presumably this can be made small as well. We will include only the principal loss mechanisms in reckoning SR .

7.1 Aerodynamic drag

Usually one estimates aerodynamic forces using the formula

$$F_D = \frac{1}{2}\rho V^2 A_f C_D \quad (8)$$

where ρ is the air density, V the speed, A_f the frontal area, and C_D the so-called drag coefficient. Normalising by m , g , and l_O gives the contribution to specific resistance:

$$\frac{F_D}{mg} = \frac{1}{2} \frac{V^2}{gl_O} \frac{\rho A_f l_O}{m} C_D \quad (9)$$

The first RHS quotient is just the square of the normalised speed as in figure 3. The second quotient is the normalised mass of the cube of air roughly enclosing the model. On Earth this number is of order 0.01. Finally [Hoerner 65] suggests $C_D \approx 1$ for a human. The aerodynamic contribution to SR then amounts to about 0.01 in a jog, and 0.05 in a sprint ($V = 3.5$). These figures are similar to estimates made by [Margaria 76] from experimental data. Considerable improvement could be realised by streamlining, and so reducing C_D .

7.2 Landing impulses

Foot-strike impulses cause dissipation in bipeds with asymmetric running cycles or nonzero foot mass. The energy loss due to nonzero foot mass may be estimated by imagining a point mass m_f hitting the ground with speed v_{foot_T} and stopping instantaneously. Then

$$\Delta E = \frac{1}{2} m_f v_{foot_T}^2 \quad (10)$$

This loss is incurred once per stride. With m_f and v_{foot_T} in dimensionless form, dividing by stride length gives the contribution to SR (7). Now in a symmetric run $v_{foot_T} = -\dot{l}_{C_T}$. (That is, landing is the mirror image of take-off, and at take-off the foot moves parallel to the leg axis.) Hence

$$\frac{\Delta E}{s} \approx m_f \frac{\dot{l}_{C_T}^2}{2s} \quad (11)$$

Even in a sprint $\dot{l}_{C_T}^2/2s < 1$, so at most the contribution of unsprung mass to specific resistance is numerically equal to m_f . At slower speed it is only half that or less. For a carefully designed machine m_f can be quite small; [Raibert 86] achieved $m_f \approx 0.01$ in his quadruped, even with each foot incorporating part of a pneumatic actuator. That leaves unsprung mass a very minor contributor to the total SR .

On the other hand, an effectively larger unsprung mass can be inferred for humans from measurements of the vertical component of the landing impulse. According to our model this is $\approx m_f \dot{l}_{C_T}$. Force measurements by [McMahon 87] indicate a value of ≈ 0.08 at $V \approx 1.4$. At this speed $\dot{l}_{C_T} \approx 1$, so $m_f \approx 0.08$. We presume that the apparently high unsprung mass is due to the leg having a knee rather than a telescopic joint. A rotating joint transmits impulses; a sliding joint cannot.

If the cycle is asymmetric, then there is additional impulsive loss even with zero unsprung mass. For example, the cycles of figure 9 are made asymmetric by stance damping; the foot lands with nonzero speed in the direction normal to the leg, and an impulse occurs. But usually, as in this case, the impulse dissipates only a small amount of energy. The loss becomes appreciable only in a cycle made unusually asymmetric, for example by a large offset between the leg axis and mass centre (figure 11).

7.3 Joint friction

The final dissipation mechanism is friction in the stance leg and hip joint. This can be expressed by a damping ratio, as in figure 9. Consider first the stance compression. Data presented by [Raibert 84] indicate the practical possibilities; his monopodal hopper with its pneumatic stance spring achieved a damping ratio of 0.06. Figure 10 shows the consequences for a bipedal runner. Substantial improvement could be realised by using a metallic spring rather than a pneumatic cylinder (but at the price of non-adjustable stiffness). Most likely one would then be left with the telescopic bearings as the limiting factor; these need sufficient strength to carry impulsive loads normal to the leg axis.

Meanwhile damping at the hip joint requires special attention, since its consequences are not limited to a simple increase in SR . Figure 11 shows that damping added to an otherwise symmetric run makes the foot land with excess forward speed. Instantaneous stopping of the foot would then require an impulsive *pull* from the floor. (Actually this is a physical impossibility, but that's not really the point since instantaneous stopping is still not a bad approximation; cf. §11.) The problem, as one might imagine, is that a pull verges on tripping, and if hip damping is increased beyond a small upper limit that is exactly what happens. The cycle vanishes.

Actually a similar problem arises in walking, and fortunately, as in walking, there is a simple remedy [McGeer 88]. Figure 11 shows that the cycle is restored by an offset (w) between the leg axes and mass centres. Simply put, offset adds negatively to v_{foot_T} at landing, and hip damping positively. By balancing one against the other, one can make v_{foot_T} just right, and so eliminate the landing impulse. This is the optimal situation, since while excess offset provides a safety margin against the dangers of hip damping, it also introduces a positive impulse. The impulse increases SR and moreover tends to destabilise the totter mode.

Of course the best strategy is to attack the root of the problem and keep the hip damping small. Our walking machines offer a case study. Our original gravity-powered walker had free ball bearings in the hip joint, which made for very low friction and no need for offsetting of the mass centres. The new actively-powered walker has presented a more difficult design problem, since each hip must include an actuator for both torso stabilisation and step-to-step modulation of the walking cycle. Friction and inertia introduced by the actuators must be kept small, which rules out the usual methods of first resort, *i.e.* hydraulics or DC motors driving reduction gears. After much brainstorming and travail we hit upon using antagonistic tendons pulling cranks on either side of the joint. Torque is varied by differential adjustment of the crank radii, while with equal radii and appropriate tensioning of the tendons, the net torque can be kept quite small regardless of the torso/leg angle. With this scheme we expect to limit the hip damping ratio to order 0.01.

For a running machine the design problem is actually simpler, since the hip need not reduce to a free pin joint. One can use a mechanical spring, with an actuator in series to set the equilibrium angle and so control the torque. We expect that damping could be at least as small as in our walking machine, and the contribution to specific resistance would then be less than 0.01 (figure 11).

7.4 Total specific resistance

Table 3 summarises our “probably conservative” estimates for the various contributions to the specific resistance of running. These confirm, as the jogger already knows, that despite the promise of the conservative model practical running is indeed much harder than walking. Not only is the SR much higher, but power ($resistance \times speed$) is higher still. For example, in sprinting at $V = 3.5$ our estimate for the normalised power is about 0.6; in walking it is only about 0.003. The normalising factor for power is $mg\sqrt{g/l_0}$ or ≈ 3 horsepower for a human; thus a human-sized sprinting machine would need at least a 2 horsepower engine.

Table 3: “Probably conservative” estimate of specific resistance in running

MECHANISM	PARAMETER	RESISTANCE			MEANS FOR IMPROVEMENT
		jogging	running	sprinting	
aerodynamic drag	C_D	0.01	0.03	0.06	streamlining
unsprung mass	m_f	< 0.005	< 0.005	0.01	structural design
normal impulse	asymmetry	< 0.005	< 0.005	< 0.005	symmetry
stance damping	d_{leg}	0.05	0.07	0.10	efficient leg spring, bearings
hip damping	d_{hip}	< 0.005	0.01	0.01	efficient hip spring, bearings
foot slip	μ	< 0.005	< 0.005	< 0.005	high traction
TOTAL	SR	0.06	0.11	0.18	

Of course one can hardly resist comparing these estimates of what a machine might achieve to performance in human running. [Margaria 76] shows measurements of energy consumed while running on a treadmill (and so without aerodynamic drag) which indicate an “overall” SR of 0.43 (i.e. with chemical energy in the numerator of (7)). This figure is independent of speed in the range $0.8 < V < 1.9$ (fast jogging and below). Margaria also suggests an “engine” efficiency of 0.25 for muscle, which implies a mechanical SR very close to our estimates for a machine. We find the coincidence rather surprising, since a human has all of the losses which we have considered already, plus some metabolic cost in “synthesising” the leg and hip springs. The implication is that either the spring synthesis is very economical, or we have been rather too conservative in our SR estimation.

(It is interesting to note that while SR ’s appear to be quite similar in “human” and “machine” running, the figures are not so close for walking. Margaria’s data indicate a “mechanical” SR of ≈ 0.05 in human walking; [Waldron 84] quotes ≈ 0.08 . The figure for our gravity-powered biped is only half as large.)

8 “Active” energy supply

Consider now means other than steady descent for overcoming the specific resistance. There are two obvious alternatives for energy supply: thrust with the stance leg, or apply torque about the hip. Hip torque turns out to be more attractive, and we will discuss this method first. Unfortunately it can supply only a limited amount of energy; for more power one can use stance thrusting, which requires a bit more care but is still satisfactory.

8.1 Stance/torso torque

Suppose that during contact a torque T_T is applied to the stance leg, *in addition to* the torques due to the hip spring and gravity. This new component does additional work on the leg, and so adds energy to the cycle amounting in symmetric running to $2T_T\theta_{C_T}$. The cycle might therefore be sustained on some slope, say γ , different from that for steady running, say γ_P . An energy balance implies that

$$2T_T\theta_{C_T} \approx s(\gamma_P - \gamma) \quad (12)$$

Solving for T_T required to run on slope γ leaves

$$T_T \approx \frac{s}{2\theta_{C_T}}(\gamma_P - \gamma) \quad (13)$$

Note that one specifies speed via γ_P ; the higher the speed, the larger γ_P (figure 10), and the more T_T is required to sustain the cycle on slope γ .

We deliberately said only that steady running *might* be possible on this slope; the energy balance must apply if a cycle exists, but it doesn't guarantee existence! However in this case there is no need to quibble, since indeed cycles do exist as plotted in figure 12. In fact varying T_T changes almost nothing about the cycle *except* the slope. Moreover the totter eigenvalues move a little in the stabilising direction. So energy input by stance torque is a method promising unblemished goodness.

The only problem is that torque has to be produced by pushing against something. The swing leg is the obvious partner, but its relatively low inertia proves inconvenient. Calculations with a reaction torque applied to the swing leg indicate rapid deterioration of symmetry and totter stability with increasing T_T . A better alternative is to push against a leaning torso whose centroid is a distance c_T from the hip. Thus if the torso is held at angle θ_T (measured from the surface normal) by reaction against the stance leg, then the (normalised) torque felt by the leg is

$$T_T = m_T c_T \sin(\theta_T + \gamma) \quad (14)$$

The torso angle required for running on slope γ therefore satisfies, from (13),

$$\sin(\theta_T + \gamma) \approx \frac{s}{2m_T c_T \theta_{C_T}}(\gamma_P - \gamma) \quad (15)$$

For illustration, take $c_T = 0.3$. Then with parameters as in figure 12 this works out to $\theta_T/\Delta\gamma \approx 9$ for small angles. It is hard to imagine leaning the torso even so much as 1 rad, so in this example one could achieve steady running only on slopes within $\pm 0.1 \text{ rad}$ of γ_P . It is also hard to imagine making the sensitivity to torso angle much larger than in this example, so for steeper slopes another scheme is required.

8.2 Stance thrust

The alternative is to thrust with the stance leg, which can be done in any number of ways. One simple option would be negative damping, *i.e.* an incremental force proportional to l_C .

This is unattractive, however, because just as positive damping improves the stability of the totter mode (figure 9), so negative damping degrades stability. A more promising option turns out to be "ramping" the relaxed position of the stance spring, according to

$$l_{zf} = l_0 + l_\theta \theta_C \quad (16)$$

The energy supplied can be estimated as follows. Since over one cycle there is no net vertical acceleration, the average vertical force during stance must be $mg\tau_0/\tau_c$. Multiplying by the change in equilibrium stance length gives an estimate of the work done. Thus the value of l_θ required for steady (symmetric) running would satisfy

$$mg \frac{\tau_0}{\tau_c} l_\theta 2\theta_{CT} \approx mg s (\gamma_P - \gamma) \quad (17)$$

Hence

$$(\gamma_P - \gamma) \approx \frac{2\theta_{CT}}{\tau_c} \frac{\tau_0}{s} l_\theta \quad (18)$$

But

$$\frac{2\theta_{CT}}{\tau_c} \approx \Omega_{CT} \approx V \quad (19)$$

and

$$\frac{s}{\tau_0} = V \quad (20)$$

Thus (18) reduces to

$$(\gamma_P - \gamma) \approx l_\theta \quad (21)$$

Exact cycle calculations (Figure 13) validate this estimate. Actually l_θ turns out to be about one-third again more powerful than indicated by (21); the error in approximation arises mainly because $\Omega_{CT} > V$ (19). Another factor is that stance thrusting reduces the landing impulse. The effect on energetics is relatively small, but the implications for cycle dynamics are substantial. Sufficiently large l_θ makes the impulse negative, and the cycle trips. This would limit the climb gradient, but as with hip damping (figure 11) w (i.e. mass centre offset) comes to the rescue. Actually humans may use the same compensation technique. When running on the level we let support roll all the way from heel to toe, but when climbing we run only on our toes. In effect this makes w negative, since the leg's mass centre moves backward with respect to an axis connecting support point and hip.

Thus with appropriate use of l_θ and mass offset, running can be regulated over a wide range of slopes. Figure 14 shows a pair of examples. The cycles are much the same, except for a 17% difference in gradient. They also differ somewhat in leg trajectories, though not so much as might at first appear. Remember that in our convention angles are measured from the surface normal. To measure from the vertical instead one would have to shift the zero 0.17 rad between the two plots in figure 14; this would make them almost identical.

We have now studied three distinct methods for supplying energy to the running cycle: steady descent, stance/torso torque, and stance thrust. The range of options is permitted by natural robustness in the passive running dynamics. Energy is accepted in whatever form is convenient to provide and channelled into the running motion. Thus running is like pumping of a swing; nature does most of the work, and relieves the controller of any exacting demands.

9 Active stabilisation and foot placement

The utility of stance/torso torque and stance thrusting is not limited to steady running. They can also be varied "actively" from one step to the next. Such active control is useful both to accelerate recovery from disturbances and to modulate the running cycle, for example while crossing unevenly-spaced stepping stones.

An analytical framework for step-to-step modulation is provided by a linearised form of the stride function \vec{S} (*cf.* (3)). For control one includes gradients with respect to l_θ and T_T . Thus define

$$\nabla_c \vec{S} \equiv \left[\frac{\partial \vec{S}}{\partial l_\theta} \frac{\partial \vec{S}}{\partial T_T} \right] \quad (22)$$

Including these control derivatives in the linearised S-to-S equations (*cf.* (6)) leaves

$$\begin{bmatrix} \Delta\theta_{C_T} \\ \Delta\theta_{F_T} \\ \Delta\Omega_{C_T} \\ \Delta\Omega_{F_T} \\ \Delta i_{C_T} \\ \Delta v_{foot_T} \end{bmatrix}_{n+1} \approx \nabla \vec{S} \begin{bmatrix} \Delta\theta_{C_T} \\ \Delta\theta_{F_T} \\ \Delta\Omega_{C_T} \\ \Delta\Omega_{F_T} \\ \Delta i_{C_T} \\ \Delta v_{foot_T} \end{bmatrix}_n + \nabla_c \vec{S} \begin{bmatrix} \Delta l_\theta \\ \Delta T_T \end{bmatrix}_n \quad (23)$$

This set of equations is in standard form for the linear-quadratic regulator algorithm. (Readers unfamiliar with this technique may wish to consult a text such a [Bryson 75]). As an example, take the cycle of figure 2, which has an *unstable* totter mode (Table 2). Thus although the cycle is generated passively, it must be stabilised *actively*. Its gradient matrices are as follows. Note that there are only 5 state variables, since sliding is disallowed.

$$\nabla \vec{S} = \begin{bmatrix} -1.36 & 0.002 & 0.01 & 0.013 & 0.59 \\ -1.26 & 1.39 & 0.52 & 0.70 & 0.91 \\ -1.73 & 0.47 & 0.26 & 0.27 & 1.46 \\ -6.34 & -3.37 & -2.92 & -1.49 & -0.06 \\ 0.51 & -0.67 & 0.70 & -0.38 & -0.30 \end{bmatrix} \quad (24)$$

$$\nabla_c \vec{S} = \begin{bmatrix} 1.88 & 0.12 \\ 1.16 & 6.0 \\ -0.41 & 0.85 \\ 6.27 & -0.22 \\ 3.60 & 0.32 \end{bmatrix} \quad (25)$$

We applied the LQR algorithm in 3 cases: one using only l_θ for control; one using only T_T , and one using both. In each case we weighted the control and state variables equally. The calculations revealed that T_T is relatively ineffective; unreasonably large control gains are required to stabilise the cycle. On the other hand l_θ is quite powerful. An appropriate control

law turns out to be

$$\Delta l_\theta = [-0.012 \ 0.292 \ -0.027 \ 0.147 \ 0.228] \begin{bmatrix} \Delta\theta_{CT} \\ \Delta\theta_{FT} \\ \Delta\Omega_{CT} \\ \Delta\Omega_{FT} \\ \Delta i_{CT} \\ \Delta v_{footT} \end{bmatrix} \quad (26)$$

(Since T_T has such a weak effect, the LQR algorithm effectively ignores it even if it is made available for use along with l_θ .) Notice that to implement this control law one need measure the state variables only at take-off. The motion during the rest of the step is treated as a black box whose internal operations one can simply ignore. This makes for simple implementation, and satisfactorily stable S-to-S modes as listed in table 4.

Table 4: Active stabilisation of the cycle of figure 2

mode	1	2	3	4,5	
				mag.	±phase
eigenvalue	-0.004	-0.52	0.70	0.22	± 0.44
θ_{CT}	0.06	0.03	0.05	0.19	± 0
θ_{FT}	-0.43	-0.33	0.74	0.48	± 1.15
Ω_{CT}	-0.05	0.06	-0.59	0.34	± -2.99
Ω_{FT}	0.90	0.94	-0.06	0.74	± -1.93
i_{CT}	0.06	-0.07	-0.31	0.26	± -0.10

The idea of control by modulating the steady cycle can be extended beyond stabilisation to the problem of accurate foot placement. The strategy would be to adjust l_θ or T_T during stance to control the point of landing after the subsequent flight phase. For analysis one could linearise a *landing-to-landing* stride function with respect to the state and control variables, and solve for the control necessary to produce some desired perturbation from the steady stride length. This estimate could be refined by Newton's method.

10 Large perturbations

Our stability analyses thus far have concentrated on perturbations small enough to be treated by linearisation of the stride function \tilde{S} . But not all perturbations are small. Certainly any biped can be knocked down by a sufficiently large disturbance, and disturbances of lesser magnitude will cause at least some departure from the transient predicted by linearised analysis. A question of key practical interest is, how much abuse can passive running really take? A few examples will indicate the possibilities.

Consider first an inherently stable cycle similar to those of figure 14. We did numerical experiments in which a perturbation was added to the take-off state vector, and the stride

function integrated forward over a series of steps. Perturbations in each state variable were scaled in proportion to the totter eigenvector. Since totter stability is marginal this is presumably the worst type of disturbance which one can apply. Totter eigenvalues in this case are $z = 0.96e^{\pm 2.7i}$.

Figure 15 compares two such transients, which differ by a factor of two in the amplitude of the initial perturbation. The first perturbation is sufficiently small that the transient is fit reasonably well by the linearised S-to-S equations (6). By contrast the second transient departs substantially from the linear fit, even though it shows a somewhat similar stride pattern. In fact the perturbation in the second case is just about as large as the biped can take without stumbling. The limit is about the same for perturbations in the positive and negative sense.

Both the examples of figure 15 show only slow recovery from the initial perturbation, which reflects the totter eigenvalues' proximity to unit magnitude. Accelerated convergence through active control would be desirable, and of course it is obligatory for unstable cycles such as that of figure 2. We return to that example for illustration of a transient under active control. The control law is (26), and the closed-loop S-to-S modes are those listed in table 4. Figure 16 shows a transient following an initial perturbation in proportion to the mode with the largest eigenvalue. The amplitude of the perturbation is just below the stumbling limit. If the linear S-to-S approximation (6) held, then the transient would show a simple convergence to the steady cycle with $z = 0.70$. However, the excitation in this case is sufficiently large to elicit nonlinear S-to-S effects, which excites all of the "linear" modes over the first few strides. The modes begin to emerge distinctly as the transient decays. The totter-like oscillation between the 5th and 10th strides is due to the mode with $z = -0.52$, and the mode with $z = 0.22e^{\pm 0.44i}$ is responsible for the mean decay. After the 10th stride the transient fades away in the slower $z = 0.70$ mode.

One feature of this transient may raise some doubts. In doing the calculation we specified that the stance foot comes to rest instantaneously upon landing. But on many of the strides, as shown in figure 16a, this would require a *negative* landing impulse, i.e. the ground would have to *pull* on the foot! As we mentioned in discussion of hip damping (§7) this is a physical impossibility; for a physically correct result one must account for finite friction between the ground and foot. The next section takes up this issue in detail. Here we simply present figure 16b for comparison with figure 16a; the two were calculated under identical conditions, except that in "b" the friction coefficient was specified to be 0.6 rather than ∞ . The transients are somewhat different, but there turns out to be almost no difference in the stumbling limit. Note that the transients in figure 15 also were calculated using $\mu = 0.6$.

11 Finite friction

Foot slip does not appear to be a problem in normal running, so it would seem quite reasonable to suppose that the stance foot stops instantaneously on landing. But this model can have implausible implications. As we explained in §2, if the foot lands with a nonzero velocity component normal to the leg, then instantaneous stopping calls for an impulse. Usually the impulse makes a shallow angle to the ground, so the horizontal/vertical force ratio is high

– higher than any plausible value for the friction coefficient. Moreover, as we've mentioned earlier, if the foot lands with a *forward* speed, then the vertical component of the landing impulse is *negative*. This is impossible to credit, so an explicit friction model is mandatory.

The key difference between the zero-slip and finite-friction models is in the component of the contact force normal to the stance leg. In the former case this force is simply whatever is required to keep the foot from slipping. In the finite-friction case, on the other hand, we use the coulombic model:

$$\begin{aligned} |F_y| &\leq \mu|F_x| && \text{while stationary} \\ F_y &= -\mu|F_x|\operatorname{sgn}(v_{foot}) && \text{while sliding} \end{aligned} \quad (27)$$

So long as the “stationary” condition holds, the contact forces are as for the zero-slip model. If however keeping the foot still would call for too much horizontal force, then sliding begins and the contact force is calculated as follows. Define the axial force (determined by leg length, K_{leg} , etc.) to be F_{leg} as sketched in figure 17. Then

$$F_x = F_{leg} \cos \theta_C - F_\perp \sin \theta_C \quad (28)$$

$$F_y = F_{leg} \sin \theta_C + F_\perp \cos \theta_C \quad (29)$$

Eliminating F_\perp and requiring that $F_y/F_x = \pm\mu$ leads to

$$F_x = \frac{F_{leg}}{\cos \theta_C \pm \mu \sin \theta_C} \quad (30)$$

Note that as far as this model is concerned F_{leg} is arbitrary. We choose it according to

$$F_{leg} = K_{leg}(l_{zf} - l_C) - d_{leg}\dot{l}_C \quad (31)$$

The choice of sign in (30) is determined by the direction of v_{foot} . After an interval of sliding v_{foot} may return to zero. If the stationary condition (27) then holds one switches back to the zero-slip force calculation. However it may not hold, and in that case the foot immediately starts sliding in the opposite direction. The boundary conditions may switch several times during stance, so numerical integration of the stride function must be done with care. This point is discussed in appendix E.

While the boundary conditions make for some algorithmic differences between the zero-slip and finite-friction models, for surfaces with reasonable traction the results turn out to be almost identical. Figures 18 and 19 show two examples of friction variation. The first example is conservative in the zero-slip limit. With moderate μ a brief interval of forward-then-backward sliding appears immediately after landing, but without significant effect on the running motion. (Visualisation of sliding may be aided by imagining an inverted pendulum rotating on a pin joint *vs* rotating on ice.) Effects become significant only for $\mu < 0.25$. Frictional dissipation peaks at $\mu \approx 0.1$; smaller μ leads to still more sliding, but less frictional work. We can calculate steady cycles down to very small μ , but these would be difficult to realise as instability becomes severe. This should come as no surprise to anyone who might imagine running on an ice rink!

Figure 19 uses the same model parameters except that stance damping is introduced. This leads to a landing impulse in the zero-slip case, and also calls for a downhill slope to sustain the motion. With finite friction the impulse is precluded, and instead one sees a backward-none sliding sequence with high μ , and backward-forward-none-backward with low μ . The effect on the cycle is much as in figure 18, except for a rapid increase in speed as the ground becomes slippery. Again one can imagine an ice rink, but in this case with a slope; on such a surface almost any form of passive locomotion (including sitting) is likely to have a high steady-state speed.

12 Summary of parametric effects

We have now completed a number of analyses of speed control, efficiency, stability, and energy supply. These have led us to explore variations of most parameters in our model; table 5 gives a summary of their effects. We have not yet discussed the effects of R , r_{gyr} , c , or m_T , so we will treat these here.

Table 5: Usual effects of parameter variations on the running cycle
 signs indicate the effect of a positive parameter increment
 () applies only for cycles with dissipation

parameter	τ_b	τ_c	τ_0	V	γ	stability	impulse	figure	comments
θ_{CT}	+	-	0	+	(+)	+	(+)	3, 8, 10	effective for speed control
R	-	+	0	-	(-)	-	(-)	20	foot model
r_{gyr}	0	0	0	0	0	+	(+)	21	with K_{hip} adjusted for constant ω_{sc}
c	0	0	0	0	(+)	+	(-)	22	with K_{hip} adjusted for constant ω_{sc}
w	-	-	-	+	\pm	+	-	11	compensates for d_{hip} , l_θ
m_T	0	-	-	+	(+)	+	(-)	23	with K_{hip} adjusted for constant ω_{sc}
K_{leg}	+	-	0	+	0	+	(-)	4	effective for speed control
d_{leg}	+	-	0	+	+	+	+	9	key stability parameter
K_{hip}	-	-	-	+	0	+	0	7	key stability parameter through ω_{sc}
d_{hip}	0	0	0	0	+	+	-	11	parasitic loss
l_θ	-	+	0	-	-	-	-	13, 14	energy supply, active stabilisation
T_T	0	0	0	0	-	+	-	12	energy supply through torso leaning
μ	0	0	0	0	0	0	0	18, 19	weak except on slippery ground

12.1 Foot radius

A semicircular foot allows simple modelling of translation by the point of support during the stance phase. The circular shape is relatively unimportant; the key factor is the distance travelled during stance. In symmetric running this is

$$\Delta y = 2\theta_{CT} R \quad (32)$$

For a human one might take Δy to be the distance from the heel to the ball of the foot. This is about 1/4 of the leg length, so with $\theta_{CT} = 0.6$ as in figure 4, R comes out to 0.2. (However we found that using $R = 0.1$ in figure 4 produced a better match with the human data of [McMahon 87].)

In walking foot radius strongly affects both specific resistance and stability [McGeer 89]. In running it also proves powerful. Figure 20 shows an example. Also shown in the figure is an approximation for stance time, which offers some insight into how foot radius modifies the running motion. The approximation is based on the leg-compression equation (whose exact form is (80)). With legs vertical and $\Omega_F = -\Omega_C$, the (dimensionless) equation becomes

$$\ddot{l}_C + \omega_l'^2 \Delta l_C = \omega_l' \Delta l_{eq} \quad (33)$$

where

$$\omega_l'^2 \equiv K_{leg} - \Omega_C^2 \quad (34)$$

and

$$\Delta l_{eq} \equiv \frac{1}{\omega_l'^2} [[l_O - R - (1 - m_T)(l_O - c)]\Omega_C^2 - 1] \quad (35)$$

If $\Omega_C = 0$ then this is just the equation for vertical oscillation about the equilibrium compression of the stance spring. Equilibrium in this case is as $\Delta l_{eq} = -1/\omega_l'^2$, or $-mg/K_{leg}$ in dimensional terms. But if Ω_C is nonzero, then centrifugal effect both "softens" the spring and shifts the equilibrium length upward. In fact at normal running speeds centrifugal effect is more powerful than gravity, so the equilibrium length is *greater than* l_O . Increasing R reduces the effect, and so increases the stance time as follows. Solving (33) with initial conditions $\Delta l_C = 0$, $\dot{l}_C = -\dot{l}_{CT}$ gives

$$\Delta l_C = \Delta l_{eq}(1 - \cos \omega_l' \tau) - \frac{\dot{l}_{CT}}{\omega_l'} \sin \omega_l' \tau \quad (36)$$

Stance ends when next $\Delta l_C = 0$; thus τ_c satisfies

$$\frac{1 - \cos \omega_l' \tau_c}{\sin \omega_l' \tau_c} = \frac{-\dot{l}_{CT}}{\omega_l' \Delta l_{eq}} \equiv -v_O \quad (37)$$

Solving for τ_c gives

$$\tau_c = \frac{1}{\omega_l'} \arcsin \frac{2v_O}{1 + v_O^2} \quad (38)$$

In evaluating this expression one must be careful to select the right root of \arcsin . The appropriate choice satisfies

$$\frac{\pi}{2} < \omega_l' \tau_c < \frac{3\pi}{2} \quad if \quad 1 + v_O \sin \omega_l' \tau_c < 0 \quad (39)$$

$$-\frac{\pi}{2} < \omega_l' \tau_c < \frac{\pi}{2} \quad if \quad 1 + v_O \sin \omega_l' \tau_c > 0 \quad (40)$$

Normally $\pi/2 < \omega_l' \tau_c < \pi$.

Evaluating (38) using i_{C_T} and Ω_C from the exact cycle calculation produces the “stance approximation” in figure 20. The approximation certainly isn’t perfect, but it is close enough to demonstrate that centrifugal effect is the mechanism whereby foot radius influences the running cycle. The primary result is an increase in τ_c with foot radius; this in turn has repercussions. First, if θ_{C_T} is fixed then increasing τ_c implies decreasing speed. Decreasing speed in turn is consistent with some reduction in stability. Furthermore, since $\tau_0 = \tau_c + \tau_b$ is essentially fixed by the scissor period, an increase in τ_c causes a decrease in τ_b . When τ_b becomes too small the cycle vanishes.

12.2 Leg inertia

Figure 21 shows the effect of leg r_{gyr} on the running cycle. If r_{gyr} were varied while holding all other parameters constant, then one would see a moderately strong effect attributable mostly to variation in the scissor period. However in this example we have simultaneously adjusted K_{hip} so that the scissor period remains constant. “Direct” effects of r_{gyr} then prove to be quite weak.

12.3 Leg mass centre

As with r_{gyr} the principal effect of c variation is mediated by the scissor period. If this is held constant through simultaneous adjustment of K_{hip} , then the residual effects are small. Figure 22 provides an example. The slight decrease in τ_c and corresponding increase in speed with c are due to centrifugal effect. c appears in (35) with sign opposite to R ; hence it has opposite effects on τ_c , speed, and stability.

This figure emphasizes the comparison made in §2 of the swing-recovery mechanisms in walking and running. In walking, the swing leg is brought forward by pendulum action. But in figure 22 we are changing the pendulum effect enormously (it even goes to zero with $c = 1$) yet the cycle is hardly affected at all. Thus in running swing recovery is due almost entirely to the torque applied by the hip spring. Moreover the reaction partner can be either a second leg, as in our bipedal model, or an extended torso, as in Raibert’s passive hopping model. The models look different physically, but their dynamics are the same.

12.4 Hip mass

In our model we use a point mass at the hip to provide rough accounting for the torso. As we have mentioned earlier, this has proven to be an acceptable first approximation for walking, and we presume that the same applies in running. Again in adjusting torso mass one must be careful to distinguish “direct” effects from those due to changes in the scissor period. Thus in figure 23 we have varied K_{hip} simultaneously with m_T so that ω_{sc} remains constant. The results are very similar to those of figure 22, and for good reason. m_T appears in (35) with the same sign as c , and so works through centrifugal effect in the same way.

13 Conclusion

We have now explored passive bipedal running in some variety and detail, and perhaps to the extent of overshadowing our main point. So let us finally return to the central thesis, which is that *running is simple*. It does *not* require a complex and continuous pattern of active forcing. On the contrary it can be a *passive* limit cycle. Thus under some conditions running might be sustained with no active input at all, and otherwise relatively crude methods for pumping and modulation of the natural cycle are sufficient to produce a diverse set of running motions. Calculations indicate that both the range of appropriate biped designs and the selection of control techniques are broad. The model therefore has attractive properties, and further investigation will likely improve understanding of running in man and machine.

With respect to the study of human locomotion, the central question raised by the passive model must be, do we really run like this? In view of its simple virtues one might expect passive running to be a good first approximation. Thus human running might be more fully explained by refinement of the model. First one should develop a more accurate mechanical representation, in particular with knees and better feet. Perhaps such a model would run passively with torsional springs at each joint. Marc Raibert is currently investigating this issue. The second step would be replacement of the springs with reasonable muscle and tendon models. These would allow quantitative treatment of running physiology, and perhaps suggest methods for improving performance.

If one's interest instead in machine design, then fidelity to human behaviour need not be of concern. With that in mind one should first ask whether bipedal locomotion is the right way to go. Wheels are obviously far superior for travel on relatively smooth terrain, and there are alternatives for rough terrain as well, e.g. tracks, multiple legs, and unusually large wheels. However the passive dynamic idea suggests, at least to us, that the bipedal option is favoured by nature, and in any case it has a practical advantage in specific resistance. Of course for applications in which specific resistance is important walking must be the preferred gait; running should be used only in situations requiring higher speeds or longer strides than are possible in walking.

A question of practical interest, then, involves how to design a passive biped capable of both walking and running, and how to switch between gaits. Particular attention must be given to the hip joint, which in walking must be free, and in running must have a stiff torsional spring. Moreover, a number of issues arise within the scope of running alone. Since the grand practical problem is rough-terrain locomotion, we feel that foot placement deserves special emphasis, i.e. how to land on top of a rock rather than in a hole. We have suggested one technique (§9). This must be developed, first for modulation of stride length in straight-line running; next for foot placement on "two-dimensional" rough terrain (i.e. with horizontal and vertical irregularities); and finally for roughness in 3D. A torso would have an important role as a torque-reaction partner, so this should be added to the model.

One final observation is especially important. The analytical model for running is promising, and we have shown that similar ideas for walking can be realised in practice. However, passive running has yet to be tested experimentally. Hence we feel that the next few steps should be in the laboratory.

APPENDICES

A General equations of motion

We now derive the equations of motion for the biped of figure 1. In general there are 4 equations: one pair for the two components of mass-centre translation, and another pair for rotation of the two legs. Their form changes with the boundary conditions, which may be free-flight, stance without slipping, or stance with slipping. We will first develop a set of equations which holds in general, and then specialise for each set of boundary conditions. The results are summarised in table 6.

Table 6: Equations required for evaluation of the stride function

phase	flight	non-slipping stance	slipping stance
translational	(62)	(80)	(41)
rotational	(63)	(80)	(81)
constitutive	(57)	(31), (57), (16), (13)	(31), (57), (16), (13), (27), (30)
geometric	(58), (59), (60)	(58), (59), (60), (61)	(58), (59), (60), (61), (83), (84)

Translation of the overall mass centre is governed by

$$\dot{\vec{V}}_{CM} = \vec{g} + \vec{F}_c \quad (41)$$

where \vec{F}_c is the force at the point of contact, normalised by total mass. (Also note that $g = 1$ in normalised units.) \vec{F}_c is determined by the spring force F_{leg} ; we will return to this calculation below.

Rotation of each leg is governed by an equation of the form

$$\dot{H} = T \quad (42)$$

where H is the angular momentum about the hip, and T the torque. We will do the derivation for the stance leg; the swing leg is treated similarly.

First consider the LHS. The starting point is

$$\dot{H}_C = m_{leg} \left(r_{gyr}^2 \dot{\Omega}_C^2 + \vec{r}_{HC} \times \dot{\vec{V}}_C \right) \quad (43)$$

\vec{r}_{HC} is the vector from hip to the leg's mass centre, and $\dot{\vec{V}}_C$ the acceleration at the mass centre. $\dot{\vec{V}}_C$ can be separated into components due to translation and rotation. The translational component is just $\dot{\vec{V}}_{CM}$. The rotational component is derived as follows. First, call $\vec{r}_{CM/C}$ the vector from overall mass centre to leg mass centre. This is

$$\vec{r}_{CM/C} = \vec{r}_{HC} - \vec{r}_{H/CM} \quad (44)$$

The vector from hip to overall mass centre is in turn

$$\vec{r}_{H/CM} = m_{leg}(\vec{r}_{HC} + \vec{r}_{HF}) \quad (45)$$

where m_{leg} is normalised by total mass. Thus from (44)

$$\vec{r}_{CM/C} = (1 - m_{leg})\vec{r}_{HC} - m_{leg}\vec{r}_{HF} \quad (46)$$

Differentiating for velocity gives

$$\frac{d\vec{r}_{CM/C}}{dt} = (1 - m_{leg})\Omega_C \times \vec{r}_{HC} - m_{leg}\Omega_F \times \vec{r}_{HF} \quad (47)$$

where the Ω vector points into the page in figure 1. Differentiating again leaves the component of $\dot{\vec{V}}_C$ due to rotation:

$$\frac{d^2\vec{r}_{CM/C}}{dt^2} = -(1 - m_{leg})\vec{r}_{HC}\Omega_C^2 + m_{leg}\vec{r}_{HF}\Omega_F^2 + (1 - m_{leg})\dot{\Omega}_C \times \vec{r}_{HC} - m_{leg}\dot{\Omega}_F \times \vec{r}_{HF} \quad (48)$$

Substituting this into the formula for H_C (43) completes the LHS of the rotational equation for the stance leg (42):

$$\begin{aligned} \dot{H}_C &= m_{leg}(r_{gyr}^2 + (1 - m_{leg})|\vec{r}_{HC}|^2)\dot{\Omega}_C - m_{leg}^2\vec{r}_{HC} \cdot \vec{r}_{HF}\dot{\Omega}_F + \\ &\quad m_{leg}^2\vec{r}_{HC} \times \vec{r}_{HF}\Omega_F^2 + m_{leg}\vec{r}_{HC} \times \dot{\vec{V}}_{CM} \end{aligned} \quad (49)$$

Now turn attention to the torques on the RHS of (42). Components are due to gravity, contact force, and the hip spring. The gravitational component is

$$\vec{T}_{gC} = m_{leg}\vec{r}_{HC} \times \vec{g} \quad (50)$$

The component due to the contact force is

$$\vec{T}_c = -\vec{r}_{PH} \times \vec{F}_c \quad (51)$$

where \vec{r}_{PH} is the vector from contact point to hip. Adding these two components together with a torque T_{hip} from the hip spring gives a total of

$$\vec{T}_C = m_{leg}\vec{r}_{HC} \times \vec{g} - \vec{r}_{PH} \times \vec{F}_c + T_{hip} \quad (52)$$

Usually it is convenient to eliminate \vec{F}_c in favour of $\dot{\vec{V}}_{CM}$ using (41); then

$$\vec{T}_C = (\vec{r}_{PH} + m_{leg}\vec{r}_{HC}) \times \vec{g} - \vec{r}_{PH} \times \dot{\vec{V}}_{CM} + T_{hip} \quad (53)$$

Combining this result with the angular momentum (49) completes the rotational equation of motion (42) for the stance leg. As we mentioned a similar derivation applies for the swing leg; together the pair of equations is as follows. Define

$$I_H \equiv m_{leg}(r_{gyr}^2 + (1 - m_{leg})|\vec{r}_{HC}|^2) \quad (54)$$

$$I_X \equiv -m_{leg}^2\vec{r}_{HC} \cdot \vec{r}_{HF} \quad (55)$$

Then

$$\begin{bmatrix} I_H & I_X \\ I_X & I_H \end{bmatrix} \begin{bmatrix} \dot{\Omega}_C \\ \dot{\Omega}_F \end{bmatrix} + \begin{bmatrix} 0 & m_{leg}^2 \vec{r}_{HC} \times \vec{r}_{HF} \\ m_{leg}^2 \vec{r}_{HF} \times \vec{r}_{HC} & 0 \end{bmatrix} \begin{bmatrix} \Omega_C^2 \\ \Omega_F^2 \end{bmatrix} = \begin{bmatrix} (\vec{r}_{PH} + m_{leg} \vec{r}_{HC}) \times (\vec{g} - \dot{\vec{V}}_{CM}) \\ m_{leg} \vec{r}_{HF} \times (\vec{g} - \dot{\vec{V}}_{CM}) \end{bmatrix} + \begin{bmatrix} T_{hip} \\ -T_{hip} \end{bmatrix} \quad (56)$$

Usually we choose T_{hip} according to

$$T_{hip} = K_{hip}(\theta_F - \theta_C) + d_{hip}(\Omega_F - \Omega_C) \quad (57)$$

Additional torques may be applied to one or both legs. For example, T_T in §8 is added to the first equation only.

The (x, y) components of the vectors in (56) are as follows:

$$\vec{g} = \begin{bmatrix} -\cos \gamma \\ \sin \gamma \end{bmatrix} \quad (58)$$

$$\vec{r}_{HC} = (l_O - c) \begin{bmatrix} -\cos \theta_C \\ -\sin \theta_C \end{bmatrix} + w \begin{bmatrix} -\sin \theta_C \\ \cos \theta_C \end{bmatrix} \quad (59)$$

$$\vec{r}_{HF} = (l_O - c) \begin{bmatrix} \cos \theta_F \\ \sin \theta_F \end{bmatrix} + w \begin{bmatrix} -\sin \theta_F \\ \cos \theta_F \end{bmatrix} \quad (60)$$

$$\vec{r}_{PH} = \begin{bmatrix} R \\ 0 \end{bmatrix} + (l_C - R) \begin{bmatrix} \cos \theta_C \\ \sin \theta_C \end{bmatrix} \quad (61)$$

B Flight phase

During the flight phase the contact force is zero, so the translational equations become simply

$$\dot{\vec{V}}_{CM} = \vec{g} \quad (62)$$

Meanwhile, since $\vec{g} - \dot{\vec{V}}_{CM} = 0$, the rotational equations become

$$\begin{bmatrix} I_H & I_X \\ I_X & I_H \end{bmatrix} \begin{bmatrix} \dot{\Omega}_C \\ \dot{\Omega}_F \end{bmatrix} + \begin{bmatrix} 0 & m_{leg}^2 \vec{r}_{HC} \times \vec{r}_{HF} \\ m_{leg}^2 \vec{r}_{HF} \times \vec{r}_{HC} & 0 \end{bmatrix} \begin{bmatrix} \Omega_C^2 \\ \Omega_F^2 \end{bmatrix} = \begin{bmatrix} T_{hip} \\ -T_{hip} \end{bmatrix} \quad (63)$$

The scissor mode is obtained by introducing a linear spring (57) on the RHS and linearising the dynamics for small perturbations about legs-parallel. The result is that

$$\omega_{sc} = \sqrt{\frac{2K_{hip}}{m_{leg}(r_{gyr}^2 + |\vec{r}_{HC}|^2)}} \quad (64)$$

and

$$\zeta_{sc} = \frac{\omega_{sc} d_{hip}}{2K_{hip}} \quad (65)$$

C Stance phase while not slipping

During stance the dynamics become more complicated, because the translational and rotational equations couple. However if slipping is disallowed then some of the complexity is mitigated because the order of the dynamics is reduced. Slip and slip rate are eliminated as degrees of freedom, so the translational equations can be reduced to a single scalar equation in l_C . The necessary kinematics are as follows. Take the origin of coordinates to be the contact point at midstance. Then from (45) the overall mass centre is at

$$\begin{aligned}\vec{r}_{O/CM} &= \hat{y}R\theta_C + \vec{r}_{PH} + \vec{r}_{H/CM} \\ &= \hat{y}R\theta_C + \vec{r}_{PH} + m_{leg}(\vec{r}_{HC} + \vec{r}_{HF})\end{aligned}\quad (66)$$

The first term accounts for translation due to rolling *without slipping*. To get a velocity we must differentiate, which from (61) involves

$$\frac{d\vec{r}_{PH}}{dt} = \hat{x}_C \dot{l}_C - (\vec{r}_{PH} - R\hat{x}) \times \Omega_C \quad (67)$$

\hat{x}_C is a unit vector along the axis of the stance leg,

$$\hat{x}_C = \begin{bmatrix} \cos \theta_C \\ \sin \theta_C \end{bmatrix} \quad (68)$$

Thus \vec{V}_{CM} is

$$\begin{aligned}\vec{V}_{CM} &= \frac{d\vec{r}_{O/CM}}{dt} \\ &= \hat{x}_C \dot{l}_C + \hat{y}R\Omega_C - (\vec{r}_{PH} - R\hat{x} + m_{leg}\vec{r}_{HC}) \times \Omega_C - m_{leg}\vec{r}_{HF} \times \Omega_F \\ &= \hat{x}_C \dot{l}_C - (\vec{r}_{PH} + m_{leg}\vec{r}_{HC}) \times \Omega_C - m_{leg}\vec{r}_{HF} \times \Omega_F\end{aligned}\quad (69)$$

Differentiating again gives the acceleration,

$$\begin{aligned}\ddot{\vec{V}}_{CM} &= \hat{x}_C \ddot{l}_C + \hat{y}_C 2\dot{l}_C \Omega_C - (\vec{r}_{PH} + m_{leg}\vec{r}_{HC}) \times \dot{\Omega}_C - m_{leg}\vec{r}_{HF} \times \dot{\Omega}_F - \\ &\quad (\vec{r}_{PH} - R\hat{x} + m_{leg}\vec{r}_{HC})\Omega_C^2 - m_{leg}\vec{r}_{HF}\Omega_F^2\end{aligned}\quad (70)$$

Now in the translational equations (41) we can easily compute the force *parallel* to the stance axis: it is just the spring force F_{leg} . Thus we can write that

$$\begin{aligned}\dot{\vec{V}}_{CM} \cdot \hat{x}_C &= \vec{g} \cdot \hat{x}_C + F_{leg} \\ &= -g \cos \gamma + F_{leg}\end{aligned}\quad (71)$$

The LHS, from (70), is

$$\begin{aligned}\dot{\vec{V}}_{CM} \cdot \hat{x}_C &= \ddot{l}_C - (\vec{r}_{PH} + m_{leg}\vec{r}_{HC}) \cdot \hat{y}_C \dot{\Omega}_C - m_{leg}\vec{r}_{HF} \cdot \hat{y}_C \dot{\Omega}_F - \\ &\quad ((\vec{r}_{PH} + m_{leg}\vec{r}_{HC}) \cdot \hat{x}_C - R \cos \theta_C)\Omega_C^2 - m_{leg}\vec{r}_{HF} \cdot \hat{x}_C \Omega_F^2\end{aligned}\quad (72)$$

This completes the terms in the translational equation.

Meanwhile the rotational equations (56) call for cross products involving $\dot{\vec{V}}_{CM}$. From (70) these are

$$\begin{aligned} (\vec{r}_{PH} + m_{leg}\vec{r}_{HC}) \times \dot{\vec{V}}_{CM} &= (|\vec{r}_{PH}|^2 + m_{leg}^2 |\vec{r}_{HC}|^2 + 2m_{leg}\vec{r}_{PH} \cdot \vec{r}_{HC})\dot{\Omega}_C + \\ &(m_{leg}^2 \vec{r}_{HC} \cdot \vec{r}_{HF} + m_{leg}\vec{r}_{PH} \cdot \vec{r}_{HF})\dot{\Omega}_F + (\vec{r}_{PH} + m_{leg}\vec{r}_{HC}) \times \hat{x}R\Omega_C^2 - \\ &(m_{leg}\vec{r}_{PH} \times \vec{r}_{HF} - m_{leg}^2 \vec{r}_{HC} \times \vec{r}_{HF})\Omega_F^2 + (\vec{r}_{PH} + m_{leg}\vec{r}_{HC}) \times (\hat{x}_C \ddot{l}_C + \hat{y}_C 2\dot{l}_C \Omega_C) \end{aligned} \quad (73)$$

$$\begin{aligned} m_{leg}\vec{r}_{HF} \times \dot{\vec{V}}_{CM} &= (m_{leg}\vec{r}_{HF} \cdot \vec{r}_{PH} + m_{leg}^2 \vec{r}_{HF} \cdot \vec{r}_{HC})\dot{\Omega}_C + m_{leg}^2 |\vec{r}_{HF}|^2 \dot{\Omega}_F - \\ &(m_{leg}\vec{r}_{HF} \times \vec{r}_{PH} + m_{leg}\vec{r}_{HF} \cdot \hat{y}R + m_{leg}^2 \vec{r}_{HF} \times \vec{r}_{HC})\Omega_C^2 + \\ &m_{leg}\vec{r}_{HF} \times (\hat{x}_C \ddot{l}_C + 2\hat{y}_C \dot{l}_C \Omega_C) \end{aligned} \quad (74)$$

Substituting into (56) produces the rotational equations. Define

$$I_C \equiv m_{leg}(r_{gyr}^2 + |\vec{r}_{PH} + \vec{r}_{HC}|^2) + (1 - m_{leg})|\vec{r}_{PH}|^2 \quad (75)$$

$$I_F \equiv m_{leg}(r_{gyr}^2 + |\vec{r}_{HF}|^2) \quad (76)$$

$$I_{FC} \equiv m_{leg}\vec{r}_{HF} \cdot \vec{r}_{PH} \quad (77)$$

$$I_{LC} \equiv -(\vec{r}_{PH} + m_{leg}\vec{r}_{HC}) \cdot \hat{y}_C \quad (78)$$

$$I_{LF} \equiv -m_{leg}\vec{r}_{HF} \cdot \hat{y}_C \quad (79)$$

The full set of 3 equations including (71) is

$$\begin{bmatrix} I_C & I_{FC} & I_{LC} \\ I_{FC} & I_F & I_{LF} \\ I_{LC} & I_{LF} & 1 \end{bmatrix} \begin{bmatrix} \dot{\Omega}_C \\ \dot{\Omega}_F \\ \ddot{l}_C \end{bmatrix} + \begin{bmatrix} -R(\vec{r}_{PH} + m_{leg}\vec{r}_{HC}) \cdot \hat{y} & m_{leg}\vec{r}_{HF} \times \vec{r}_{PH} \\ -m_{leg}(\vec{r}_{HF} \times \vec{r}_{PH} + R\vec{r}_{HF} \cdot \hat{y}) & 0 \\ -(\vec{r}_{PH} + m_{leg}\vec{r}_{HC}) \cdot \hat{x}_C + R \cos \theta_C & -m_{leg}\vec{r}_{HF} \cdot \hat{x}_C \end{bmatrix} \begin{bmatrix} \Omega_C^2 \\ \Omega_F^2 \\ \dot{l}_C \end{bmatrix} = \begin{bmatrix} -(\vec{r}_{PH} + m_{leg}\vec{r}_{HC}) \cdot \hat{x}_C \\ -m_{leg}\vec{r}_{HF} \cdot \hat{x}_C \\ 0 \end{bmatrix} 2\dot{l}_C \Omega_C + \begin{bmatrix} (\vec{r}_{PH} + m_{leg}\vec{r}_{HC}) \times \vec{g} \\ m_{leg}\vec{r}_{HF} \times \vec{g} \\ \hat{x}_C \cdot \vec{g} \end{bmatrix} + \begin{bmatrix} T_{hip} \\ -T_{hip} \\ F_{leg} \end{bmatrix} \quad (80)$$

D Stance phase while slipping

If slipping is allowed, then the contact force \vec{F}_c is determined from F_{leg} using the friction model (30). In this case it is most convenient to put the RHS of the rotational equations (56) in terms of \vec{F}_c rather than \vec{V}_{CM} . Using (41) the rotational equations then become

$$\begin{bmatrix} I_H & I_X \\ I_X & I_H \end{bmatrix} \begin{bmatrix} \dot{\Omega}_C \\ \dot{\Omega}_F \end{bmatrix} + \begin{bmatrix} 0 & m_{leg}^2 \vec{r}_{HC} \times \vec{r}_{HF} \\ m_{leg}^2 \vec{r}_{HF} \times \vec{r}_{HC} & 0 \end{bmatrix} \begin{bmatrix} \Omega_C^2 \\ \Omega_F^2 \end{bmatrix} = - \begin{bmatrix} (\vec{r}_{PH} + m_{leg}\vec{r}_{HC}) \times \vec{F}_c \\ m_{leg}\vec{r}_{HF} \times \vec{F}_c \end{bmatrix} + \begin{bmatrix} T_{hip} \\ -T_{hip} \end{bmatrix} \quad (81)$$

To calculate F_{leg} (31) one needs l_C and \dot{l}_C . These are determined by the condition that during stance the foot must remain in contact. That is,

$$x_{CM} - \vec{r}_{O/CM} \cdot \hat{x} = 0 \quad (82)$$

Using $\vec{r}_{O/CM}$ from (66) and solving for l_C leaves

$$l_C = \frac{x_{CM} - R - m_{leg}(\vec{r}_{HC} + \vec{r}_{HF}) \cdot \hat{x}}{\cos \theta_C} + R \quad (83)$$

Similarly, differentiating the contact condition (82) and solving for \dot{l}_C leaves

$$\dot{l}_C = \frac{\vec{V}_{CM} \cdot \hat{x} + (m_{leg} \vec{r}_{HC} \cdot \hat{y} + (l_C - R) \sin \theta_C) \Omega_C + m_{leg} \vec{r}_{HF} \cdot \hat{y} \Omega_F}{\cos \theta_C} \quad (84)$$

E Phase transition conditions

Table 7: Events triggering a switch between boundary conditions

pre → post	switching function
flight → stance	$l_C - l_{zf} = 0$ (83), (16) – foot strike
slipping → no slipping	$v_{foot} = 0$ (86) and $ F_y/F_x \leq \mu$ (41), (70)
slipping → slipping	$v_{foot} = 0$ (86) and $ F_y/F_x > \mu$ (41), (70). $\text{sgn}(v_{foot})$ changes to - $\text{sgn}(F_y)$
no slipping → slipping	$F_x - F_y/\mu = 0$ (41), (70)
stance → flight	$F_{leg} = 0$ (31) – force vanishing

Phase transitions occur under the conditions listed in table 7. To evaluate these conditions one needs expressions for v_{foot} while slipping, and for \vec{F}_c while not slipping. \vec{F}_c is found by combining the translational equation (41) with the zero-slip \vec{V}_{CM} (70). Meanwhile v_{foot} satisfies

$$v_{foot} = \hat{y} \cdot (\vec{V}_{CM} - \vec{V}_{CM/foot}) \quad (85)$$

$\vec{V}_{CM/foot}$ is given by (69) (which in the zero-slip case is just \vec{V}_{CM} .) Thus

$$v_{foot} = \hat{y} \cdot \vec{V}_{CM} - \sin \theta_C \dot{l}_C - \hat{x} \cdot (\vec{r}_{PH} + m_{leg} \vec{r}_{HC}) \Omega_C - m_{leg} \hat{x} \cdot \vec{r}_{HF} \Omega_F \quad (86)$$

E.1 Numerical search for the switching points

To evaluate the stride function (1) we start numerical integration with a fixed time step, while checking at each step the appropriate end-of-phase switching functions. (We use a fourth-order Runge-Kutta integrator, usually with time step $0.02\sqrt{l_O/g}$.) When a switching function

changes sign, we start searching the preceding interval for the “exact” switching point. For the flight→stance transition Newton’s method can be used. l_C and \dot{l}_C are easily computed (83), (84) and the estimate for switching time may be improved by

$$\Delta\tau \approx \frac{l_{zf} - l_C}{\dot{l}_C} \quad (87)$$

(This isn’t quite right if l_{zf} is a function of a time-varying θ_C (16); however the approximation proves satisfactory.)

Stance-phase transitions must be treated with more care, because the switching functions can be sharply curved. This occurs for example immediately after foot strike in the cycles of figure 18: v_{foot} can go from zero to some positive maximum and back over an interval shorter than $0.003\sqrt{l_0/g}$. Thus we use a parabolic rather than linear approximation for stance-phase switching functions. That is, when a switching function first changes sign we fit a quadratic through the last three time steps in the integration. Solving the quadratic then leaves estimates for two switching points; we choose between these roots by reference to the sense of the transition. (e.g. a forward slipping→no slipping switch must occur with $dv_{foot}/dt < 0$.) We then adjust the time step appropriately, update the quadratic fit, and continue until convergence. This technique proves effective, although some care is required to ensure a well-conditioned fit. Thus if two samples happen to fall close together, then we put the next sample at their midpoint regardless of the roots of the quadratic.

F Landing impulse

If slipping is disallowed and the foot lands with nonzero speed in the direction normal to the leg, then an impulse is required to bring the foot to rest. The impulse causes instantaneous jumps in Ω_C , Ω_F , and \dot{l}_C . Physical conditions for calculating the jumps are conservation of linear momentum parallel to the stance spring, and of angular momentum about the contact point and hip. Mathematically the linear-momentum condition is just

$$\hat{x}_C \cdot \Delta \vec{V}_{CM} = 0 \implies \hat{x}_C \cdot \vec{V}_{CM}^+ = \hat{x}_C \cdot \vec{V}_{CM}^- \quad (88)$$

The angular momentum conditions follow from the general rotational equations (56). For impulsive changes these become

$$\begin{bmatrix} I_H & I_X \\ I_X & I_H \end{bmatrix} \begin{bmatrix} \Delta\Omega_C \\ \Delta\Omega_F \end{bmatrix} = - \begin{bmatrix} (\vec{r}_{PH} + m_{leg}\vec{r}_{HC}) \times \Delta \vec{V}_{CM} \\ m_{leg}\vec{r}_{HF} \times \Delta \vec{V}_{CM} \end{bmatrix} \quad (89)$$

\vec{V}_{CM}^+ is determined by Ω_C^+ , Ω_F^+ , and \dot{l}_C^+ according to (69). Substituting here and combining with (88) leaves

$$\begin{bmatrix} I_C & I_{FC} & I_{LC} \\ I_{FC} & I_F & I_{LF} \\ I_{LC} & I_{LF} & 1 \end{bmatrix} \begin{bmatrix} \Omega_C^+ \\ \Omega_F^+ \\ \dot{l}_C^+ \end{bmatrix} = \begin{bmatrix} I_H & I_X \\ I_X & I_H \\ 0 & 0 \end{bmatrix} \begin{bmatrix} \Omega_C^- \\ \Omega_F^- \end{bmatrix} + \begin{bmatrix} (\vec{r}_{PH} + m_{leg}\vec{r}_{HC}) \times \vec{V}_{CM}^- \\ m_{leg}\vec{r}_{HF} \times \vec{V}_{CM}^- \\ \hat{x}_C \cdot \vec{V}_{CM}^- \end{bmatrix} \quad (90)$$

Note that the LHS involves the inertia matrix for the non-slipping stance equations (80), while the RHS includes the rotational inertia matrix for the free-flight equations (63).

References

- [Alexander 77] R. McN. Alexander. Mechanics and scaling of terrestrial locomotion. In *Scale effects in animal locomotion*, T. Pedley, Ed. Pergamon, Oxford.
- [Alexander 84] R. McN. Alexander. The gaits of bipedal and quadrupedal animals. *Int. J. robotics research* 3(2) 49-59.
- [Bryson 75] A. Bryson, Y-C Ho. *Applied optimal control*. Halsted Press, New York.
- [Bühler 88] M. Bühler, D. Koditschek. Analysis of a simplified hopping robot. *IEEE int. conf. robotics and automation*, Philadelphia. 817-819.
- [Hoerner 65] S. Hoerner. *Fluid dynamic drag*. Hoerner Fluid Dynamics, Brick Town, N.J.
- [Margaria 76] R. Margaria. *Biomechanics and energetics of muscular exercise*. Oxford University Press.
- [McGeer 88] T. McGeer. Stability and control of two-dimensional biped walking. *Simon Fraser University Centre for Systems Science IS-TR-88-01*.
- [McGeer 89] T. McGeer. Passive dynamic walking. To appear in *Int. J. robotics research*. June 1989.
- [McMahon 78] T. McMahon, P. Greene. Fast running tracks. *Scientific American* 239:148-163.
- [McMahon 84] T. McMahon. Mechanics of locomotion. *Int. J. robotics research* 3(2) 4-28.
- [McMahon 87] T. McMahon, G. Valiant, E. Frederick. Groucho running. *J. appl. physiol.* 62(6) 2326-2337.
- [Raibert 84] M. Raibert, H. Brown, M. Cheponis. Experiments in balance with a 3D one-legged hopping machine. *Int. J. robotics research* 3(2) 75-92.
- [Raibert 86] M. Raibert. *Legged robots that balance*. MIT Press.
- [Waldron 84] K. Waldron *et al.* Configuration design of the adaptive suspension vehicle. *Int. J. robotics research* 3(2) 37-48.

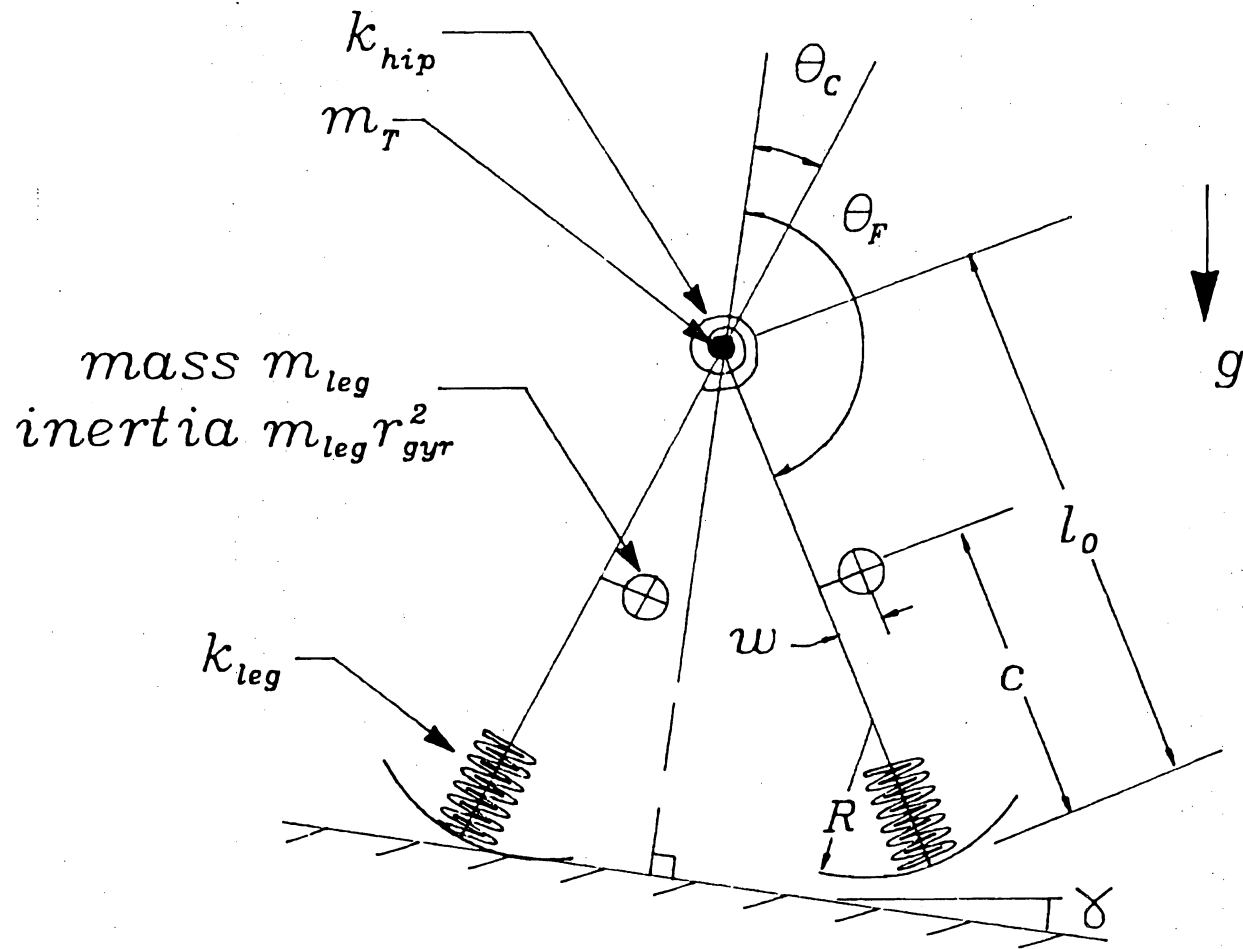


Figure 1 Running is a passive dynamic mode of this simple biped. The legs have arbitrary mass, centroid, and moment of inertia, and compress telescopically against linear springs. A torso is roughly approximated by a point mass at the hip. The feet are massless rigid semicircles. While running the legs bounce between flight and stance phases, and are cycled back and forth in a scissor motion by a torsional spring at the hip. Note that angles are measured from the surface normal rather than the vertical.

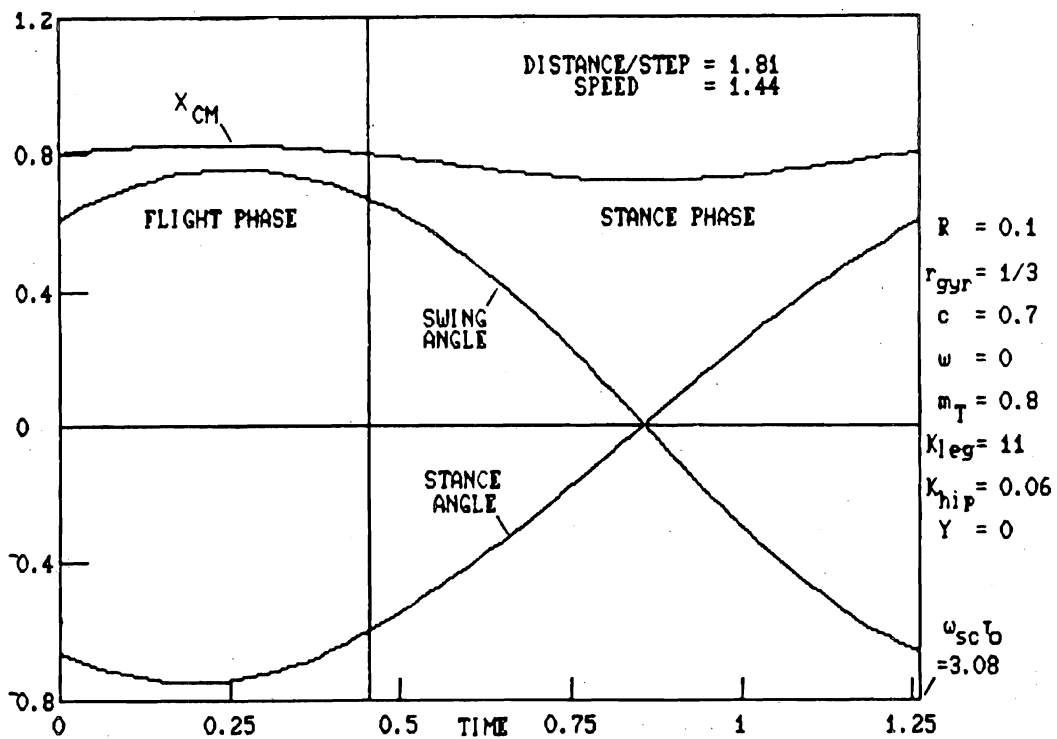


Figure 2 This example of a passive running cycle corresponds roughly to relaxed jogging in a human. It illustrates typical features of the running mode. Here all quantities are dimensionless; total mass m , nominal leg length l_0 , and gravity g provide the base units. During flight the legs first spread and then return under the influence of the hip spring; meanwhile the overall mass centre follows a parabolic free fall. Then landing compresses the stance leg, while the opposing leg swings forward. During the stance phase the swing leg is shortened as necessary to keep its foot clear. Stance rebound throws the machine off the ground, and the cycle then repeats with the legs exchanging roles. The period of one such full stride differs only slightly from the period of the legs' "free fall" scissor mode. Note that no energy is dissipated during the cycle; it is simply exchanged between kinetic, gravitational, and elastic stores. Hence the slope $\gamma = 0$.

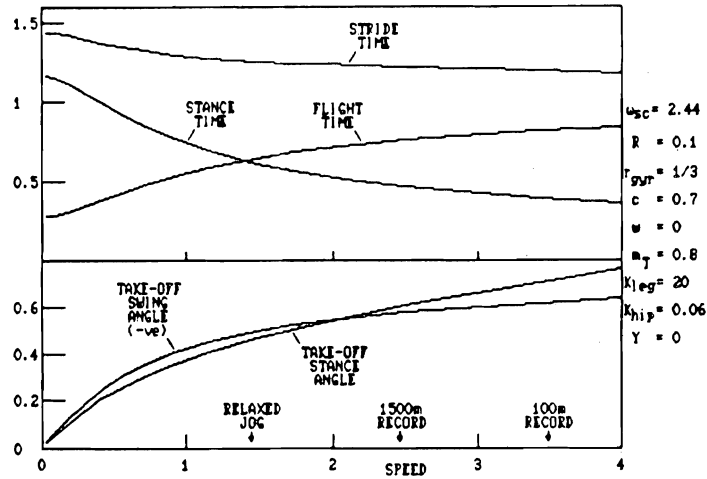


Figure 3 Increasing the amplitude of the legs' scissor action increases the running speed. Here speed is normalised by \sqrt{gO} ; the result is often called a Froude number. Humans run in the range $1 < V < 4$. ($V \approx 3.6$ is the average speed over the 100m, but the pace is faster at the end of the race.) At lower speeds walking is preferred. Notice that while the stance/flight ratio changes with speed, the time for one cycle remains nearly constant at just over half the scissor-mode period.

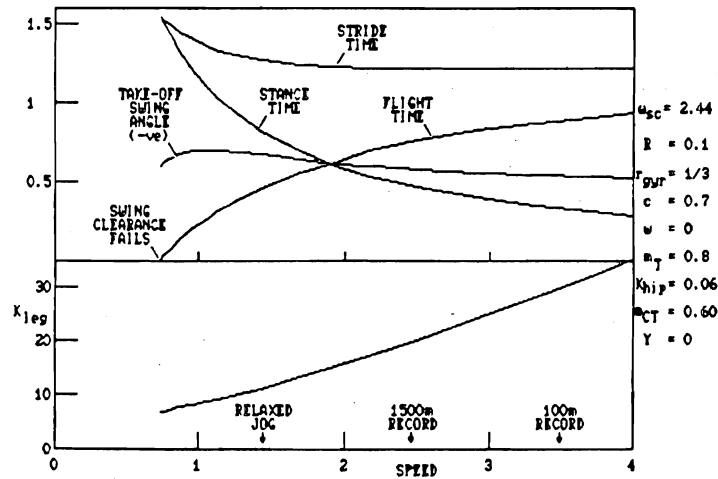


Figure 4 An alternative to controlling speed via scissor amplitude is adjustment of the stance stiffness. In this example the technique fails at low speed, because the swing leg makes contact before the stance leg can lift-off. However in the usual running range stiffness adjustment is quite effective, and in fact humans seem to use stiffness as the principal speed control. As in figure 3, the stance/flight ratio changes with speed, but the stride period stays nearly constant.

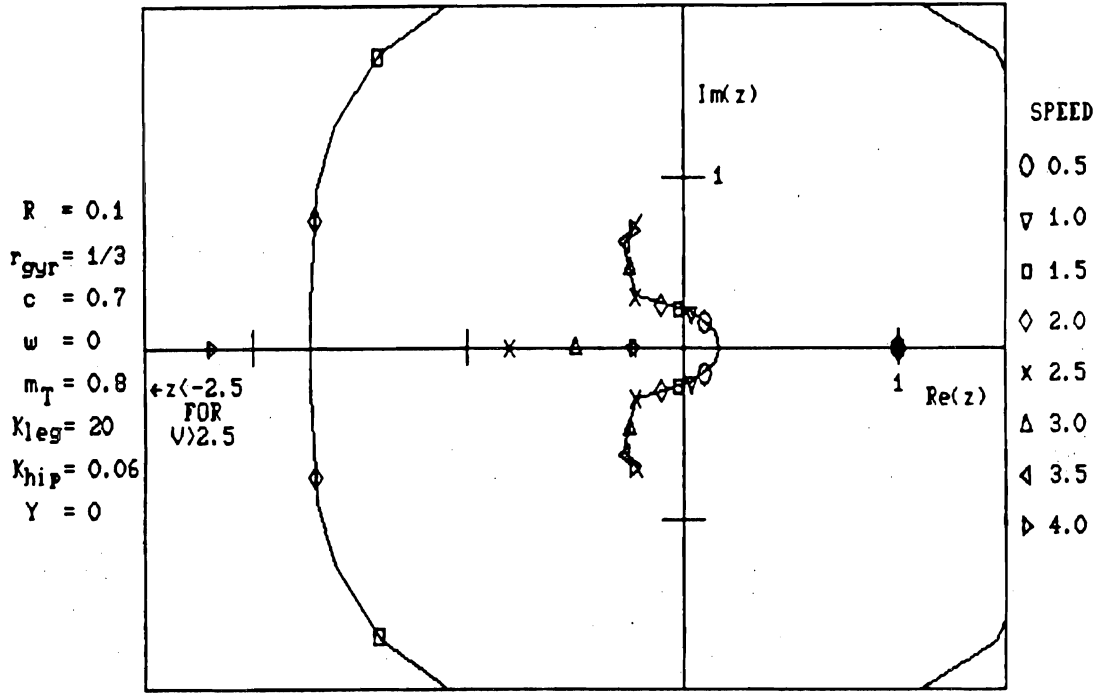


Figure 5 We are interested not only in steady running, but also in stability. A set of linearised equations ("S-to-S equations") specifies how a perturbation on the steady cycle propagates from one stride to the next. These equations have 5 modes; if z is one of the modal eigenvalues, then over n strides the amplitude of a perturbation in that mode scales with z^n . Here the positions of the 5 eigenvalues are plotted on the complex plane, in the form of a root locus vs running speed. Speed is varied via cycle amplitude, as in figure 3. One eigenvalue remains at $z = 1$ throughout the speed range; a perturbation in this mode simply shifts the steady amplitude and speed (hence this is the "speed mode"). Two more paired eigenvalues remain within the unit circle; a perturbation in this mode produces an oscillatory transient which decays quickly. Excursions are mainly in the angle of the swing leg; hence we call this the "swing mode". The final pair of eigenvalues sweeps around a broad outer arc as the speed increases, until at $V \approx 2.5$ they split left and right along the negative real axis. The split reverses as V approaches 4. Through most of the speed range this mode involves an oscillatory transient with a period of 2-3 strides; hence the name "totter" mode. In this example totter perturbations are amplified, and the mode is unstable.

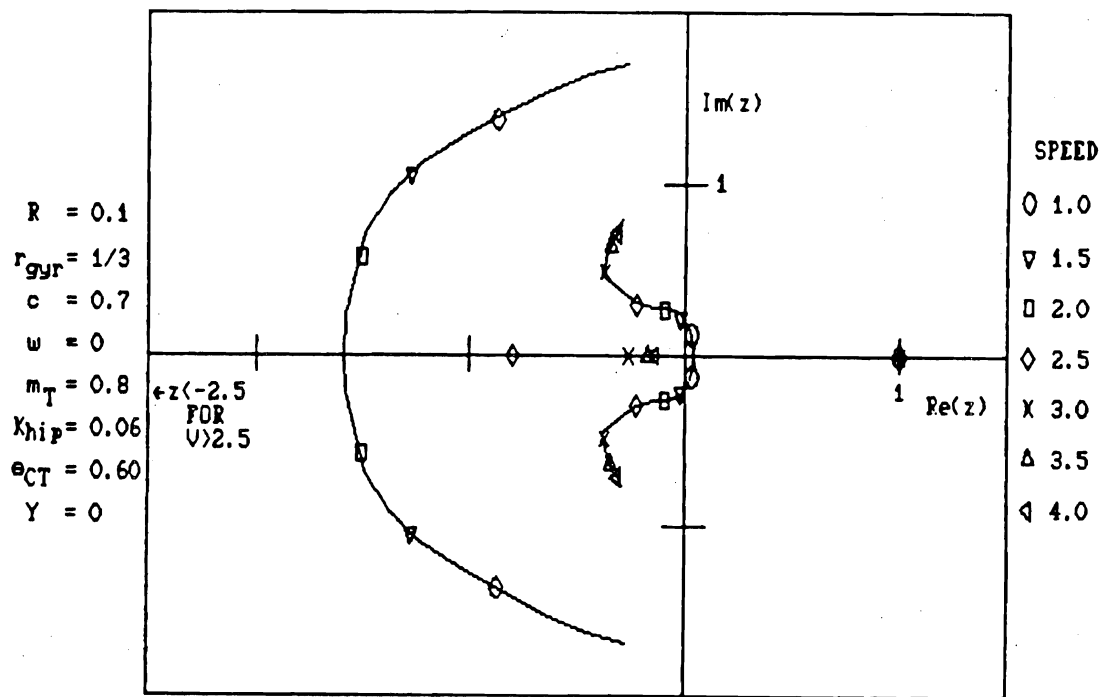


Figure 6 This is the root locus corresponding to figure 4, using stance stiffness for speed control. The pattern is much the same as in figure 5, in which cycle amplitude was the control variable. Thus the choice of speed control makes little difference to the stability of passive running.

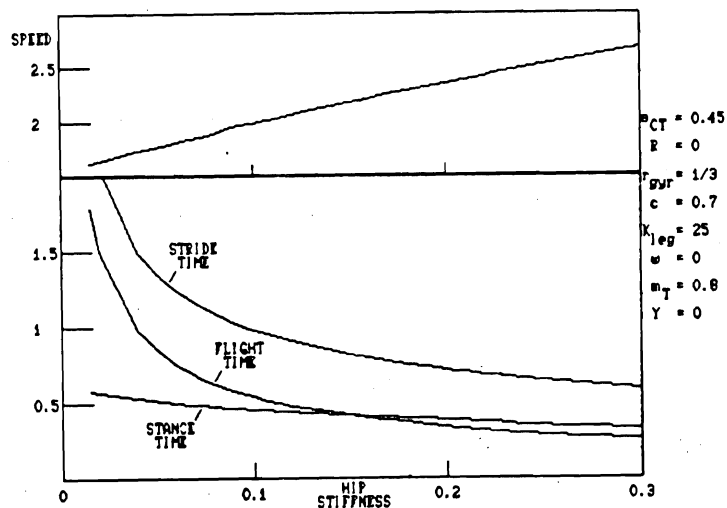
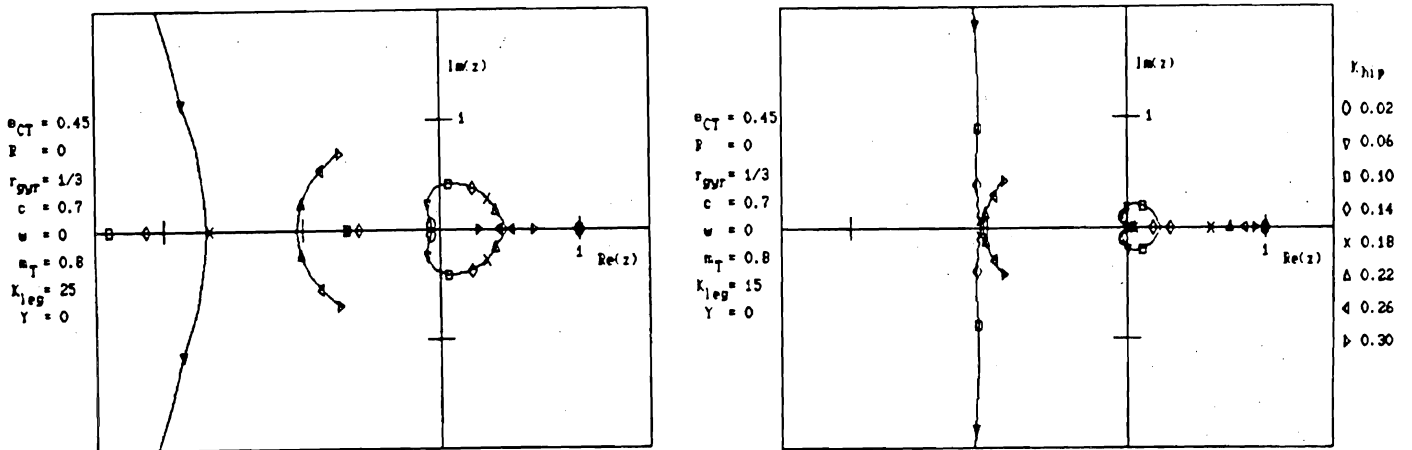


Figure 7a: Stability of the running cycle can be improved by increasing hip stiffness. In this example the totter eigenvalues converge along a broad outer locus, split along the real axis, reverse and, as K_{hip} approaches 0.22, meet near $z = -1$. They then split outward into the complex plane, closely following the arc of the unit circle. Thus with $K_{hip} > 0.22$ this cycle is neutrally stable in the totter mode, while the swing and speed modes remain well-behaved.

Figure 7b: Another example of a root locus *vs* K_{hip} , in this case with a softer stance spring. Again it shows that neutral stability can be achieved by making the hip spring sufficiently stiff.

Figure 7c: The effect of larger K_{hip} is to increase the frequency of the leg's scissor action. The scissor frequency, in turn, is nearly equal to cadence (*i.e.* the full-stride frequency). Thus cadence is a key parameter in the stability of passive running.

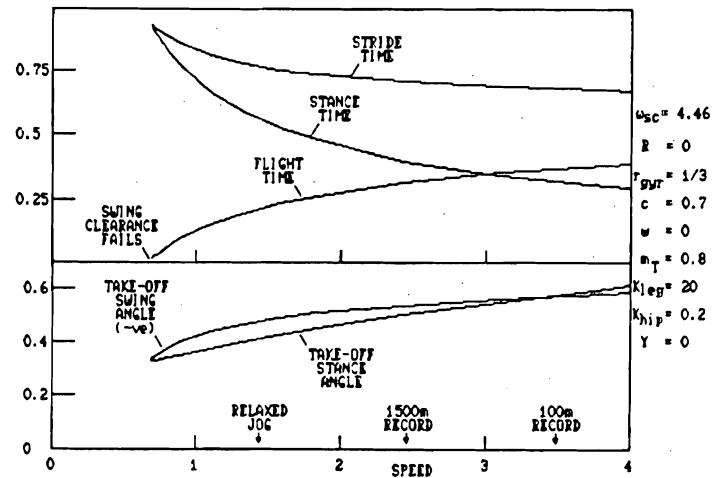
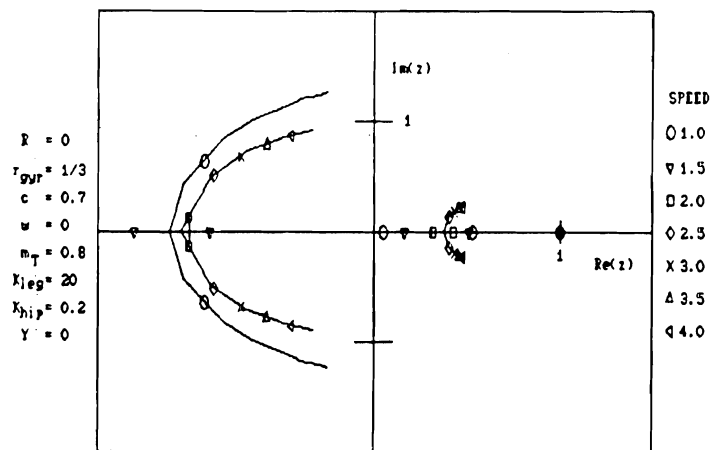


Figure 8a: This root locus emphasises features also found among the loci of figures 5, 6, and 7. In this case speed is the parameter, as in figure 5, but the hip stiffness is higher. The totter eigenvalues converge to the real axis along a broad outer arc, split left and right, rejoin again near $z = -1$, and then split again nearly along the rim of the unit circle. Thus in this example jogging is unstable, but running and sprinting have near-neutral stability. The same locus features appear regardless of whether the cycle is adjusted via θ_{CT} , as in this case, K_{leg} , or K_{hip} .

Figure 8b: Meanwhile features of the cycle show the same trend with speed as in figures 3 and 4. The cycle period is substantially shorter in this example, although about the same when expressed as a fraction of the legs' scissor period.

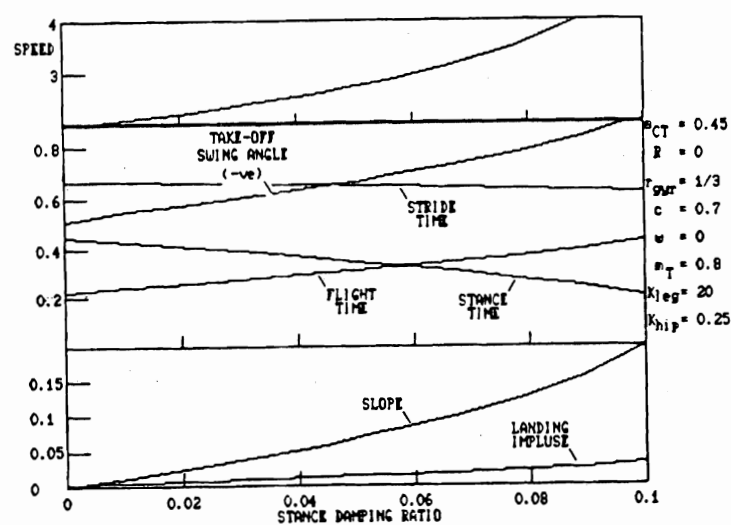
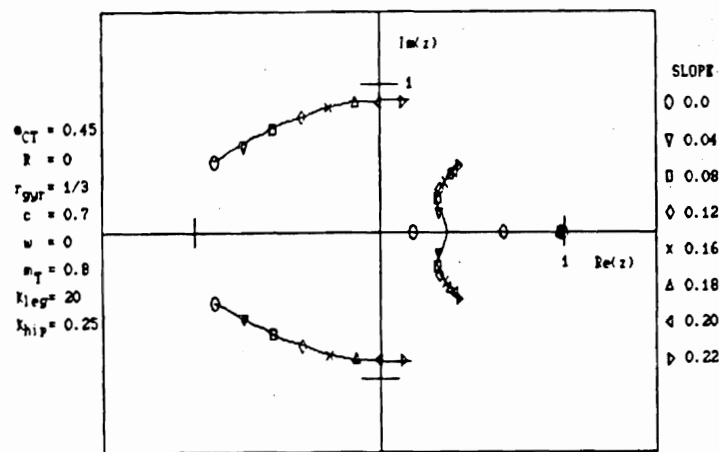


Figure 9a: The totter mode can be made absolutely stable by damping in the stance spring. However the running cycle then becomes dissipative, and losses must be recouped by (in this case) running downhill. For any given slope energy balance can be established at only one speed. Hence damping not only stabilises the totter mode, but also moves the speed eigenvalue slightly inside the unit circle.

Figure 9b: If all other cycle parameters are held constant, then as damping increases so do the slope and running speed. To maintain constant speed one would have to adjust cycle amplitude or stance stiffness simultaneously (figure 10). Damping makes the running cycle asymmetric; stopping the foot on landing then calls for an impulse. The direction of the impulse is normal to the stance leg.

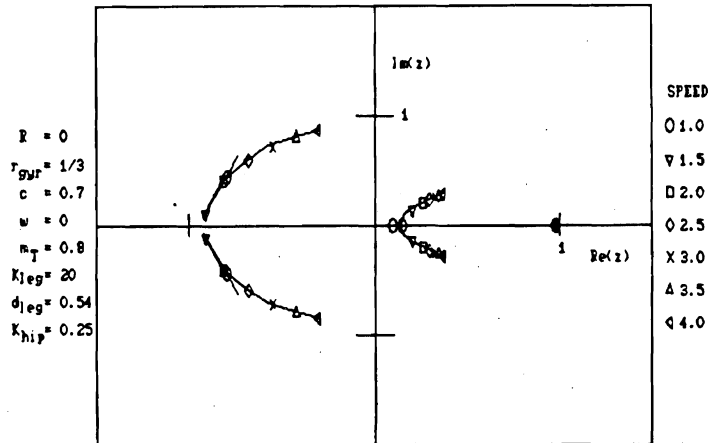
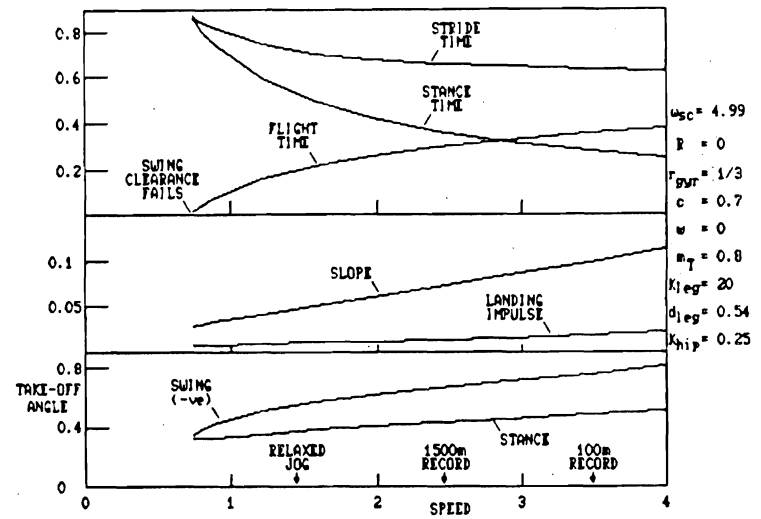


Figure 10a: In this example speed is adjusted as in figure 3, but K_{leg} and K_{hip} are chosen for better totter-mode stability. Also stance damping (d_{leg}) is introduced sufficient for a damping ratio of 0.06 (cf. figure 9). This is comparable to that achieved in Raibert's hopping machine [Raibert 84], and so represents the possibilities for a bipedal runner. For any gravity-powered vehicle the descent gradient is equal to the specific resistance, and so provides a fundamental measure of efficiency. For example, here the SR is about 10% for fast jogging. This figure is an order of magnitude larger than for normal walking.

Figure 10b: With high cadence and stance damping, passive running is stable across the whole speed range. Note that on this locus the outer and inner "totter arcs" are almost coincident.

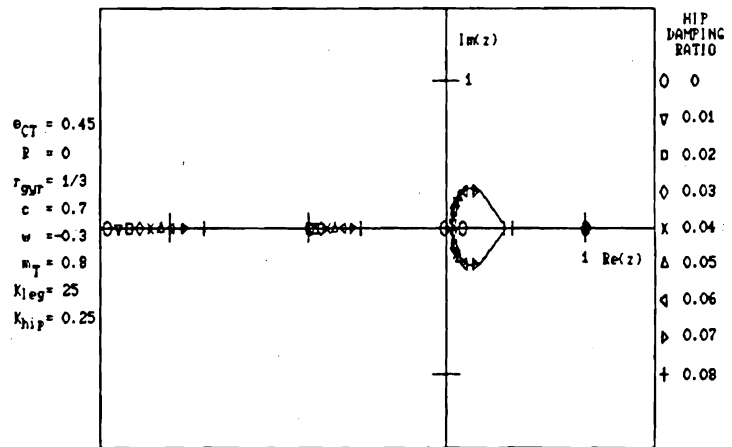
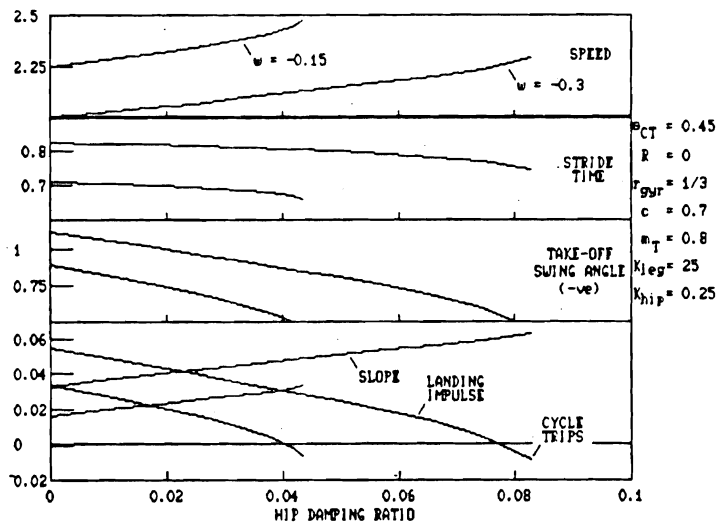


Figure 11a: While damping in the stance spring can be balanced simply by a downhill slope, damping in the hip requires more careful attention. Adding damping to an otherwise symmetric run makes the foot land with excess forward speed. Stopping the foot then calls for a negative impulse (*i.e.* a downward pull), which is not only physically impossible but also dynamically unacceptable. Thus only slight dissipation at the hip is sufficient to trip the passive cycle. The situation can be retrieved by shifting each leg's mass centre backward from the leg axis (*cf.* figure 1).

Figure 11b: While offsetting the leg mass restores passive running even with a dissipative hip joint, the solution is not completely satisfactory because offset is destabilising. Therefore low hip damping is desirable for not only efficiency but also robust cycle dynamics.

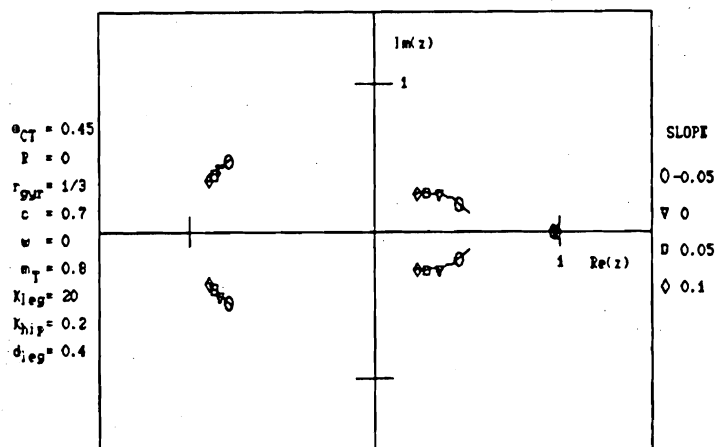
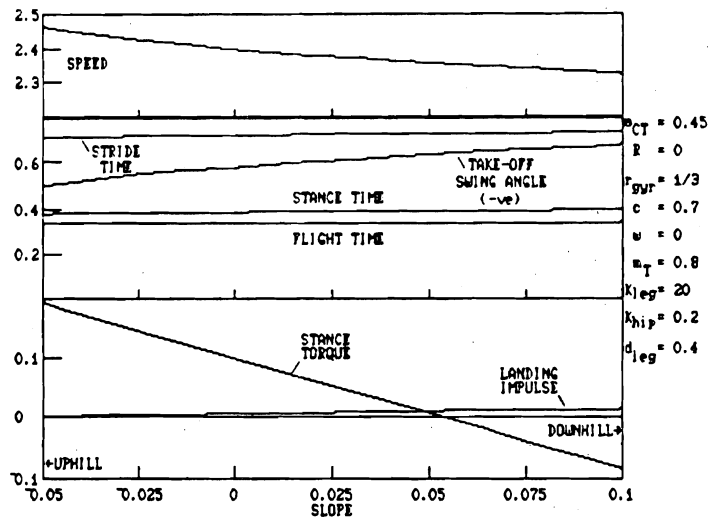


Figure 12a: Some means of "active" energy supply is required in order to replace dissipated energy, and to regulate climbs and descents. One method is to apply torque to the stance leg during the stance phase. In practice the torque can be generated by reaction against a leaning torso. This technique is attractive, because for a given set of model parameters a change in torque produces only a change in slope, with negligible effects on other features of the run. If the slope is fixed, then stance torque becomes a speed control.

Figure 12b: Stance torque also has only a small effect on stability.

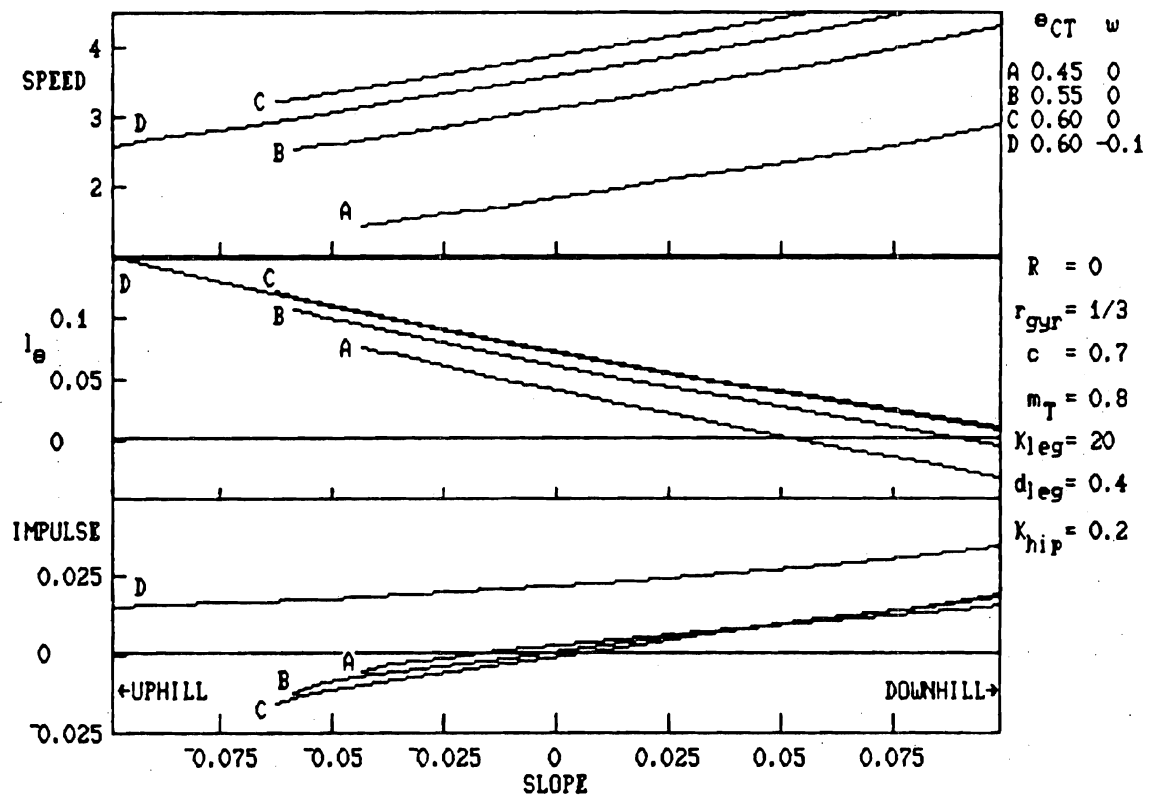


Figure 13 An alternative method of energy supply is to thrust with the stance leg. In this example the thrust is generated by "ramping" the equilibrium length of the spring, according to $l_{zf} = l_O + l_\theta \theta_C$. Some care is required when using this technique, because sufficiently large l_θ makes the landing impulse negative and so "trips" the running cycle. To compensate for this effect the legs' mass centres must be offset backward. A steeper climb requires more l_θ , and so more offset. Humans may use similar compensation: we climb hills on our toes.

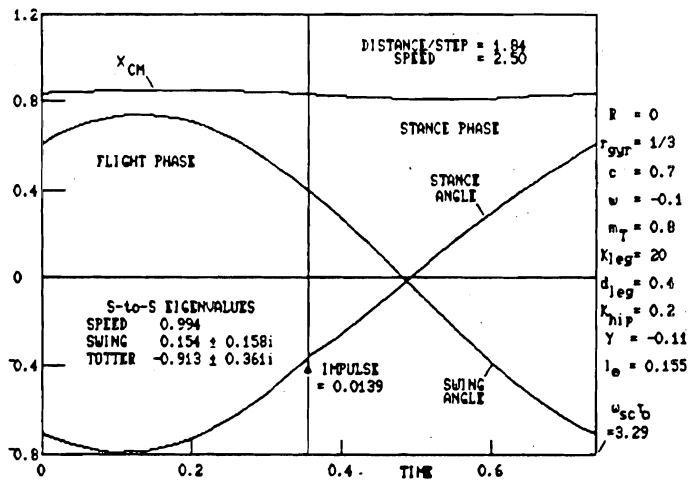
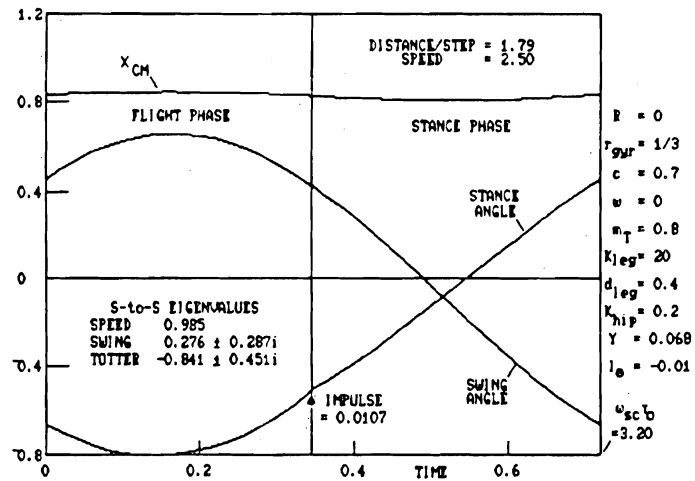


Figure 14 Two running cycles are shown for an example biped. The slopes differ by 17%, but the cycles and their stability are nearly identical thanks to appropriate control of stance thrust and leg mass offset. Note that the angles are measured from the surface normal; to measure from the vertical, shift the zero by 0.17rad between the two figures.

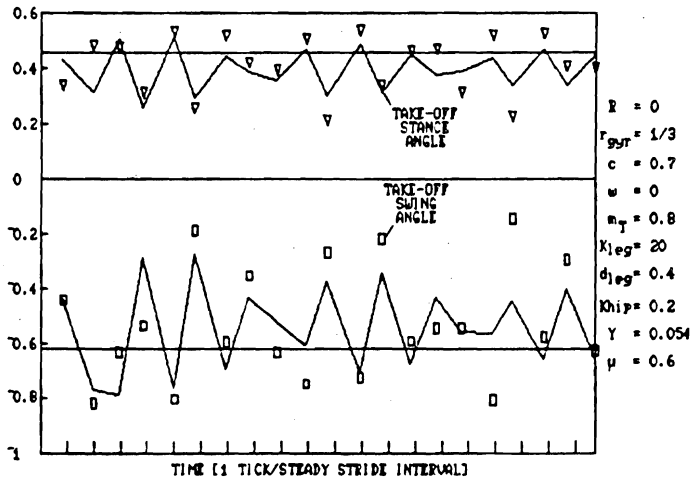
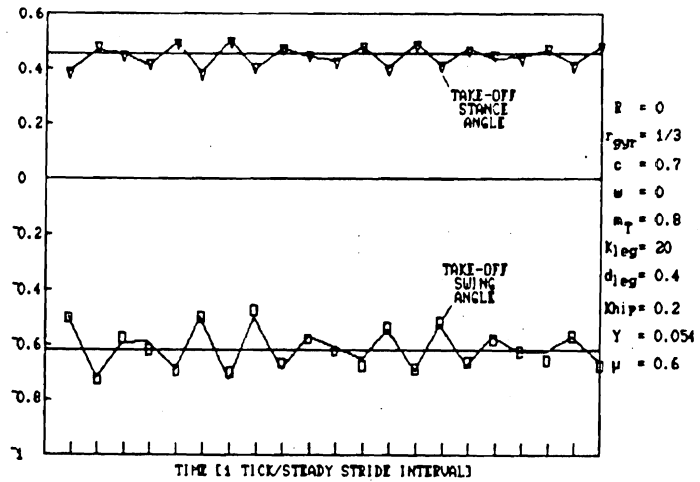


Figure 15a: This example shows the transient following an initial excitation of the totter mode. The steady cycle in this case is similar to those in figure 14, and the totter eigenvalues are $z = 0.96e^{\pm 2.7i}$. Hence the transient involves a slow oscillatory decay. Symbols show the stance and swing angles at take-off, as calculated using the exact stride function. Lines show the best fit by the linearised S-to-S equations. Two strides correspond to one full scissor of the legs. Previously we have specified zero sliding between the stance foot and ground, but this can call for anomalous contact forces during the transient (*cf.* figure 16). Hence in this example we have specified a finite friction coefficient.

Figure 15b: Here the totter-mode perturbation is twice that in the preceding example, and in fact as large as it can be without causing a stumble. The transient patterns are qualitatively similar in the two cases. However the larger perturbation is sufficient to elicit nonlinear effects in the stride function, and the S-to-S linearisation fits the transient poorly.

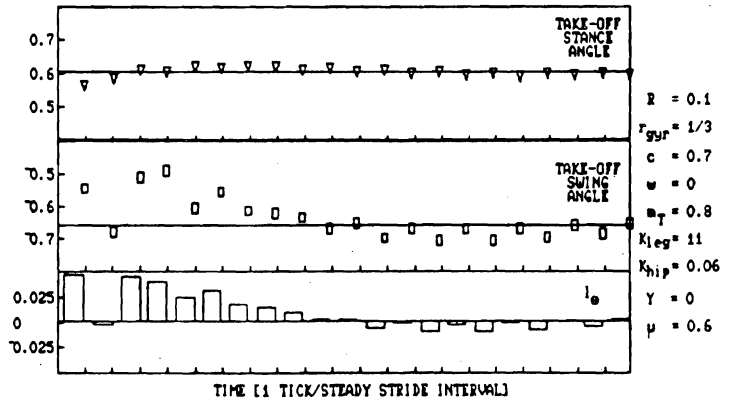
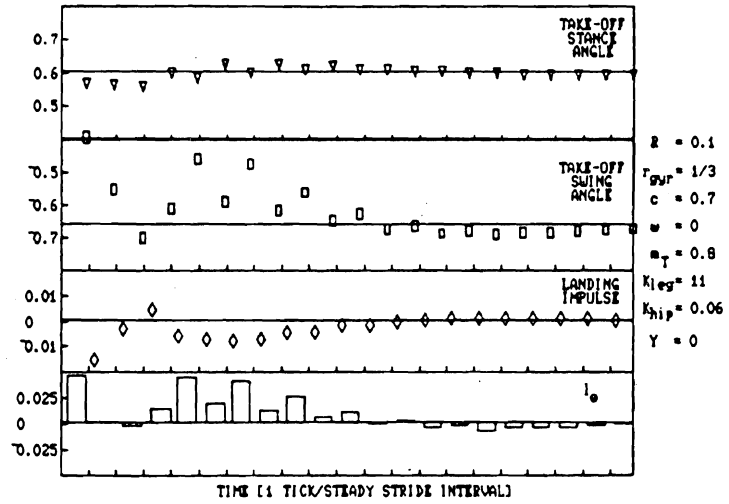


Figure 16a: Here the transient follows a perturbation on the cycle of figure 2; the amplitude of the perturbation is just below the stumbling limit. This cycle is passively unstable, so we stabilise actively via feedback adjustment of stance thrust (l_θ) as indicated. In calculating the transient we have specified that the stance foot cannot slip. This calls for a negative (*i.e.* downward) impulse on many of the landings, which is physically impossible.

Figure 16b: The problem of anomalous landing impulses is resolved by specifying finite friction between the stance foot and ground. Here the perturbation is as in the preceding example, but we have taken the friction coefficient to be 0.6. The two transients are similar, so the zero-slip model is reasonably accurate despite the nonphysical contact forces.

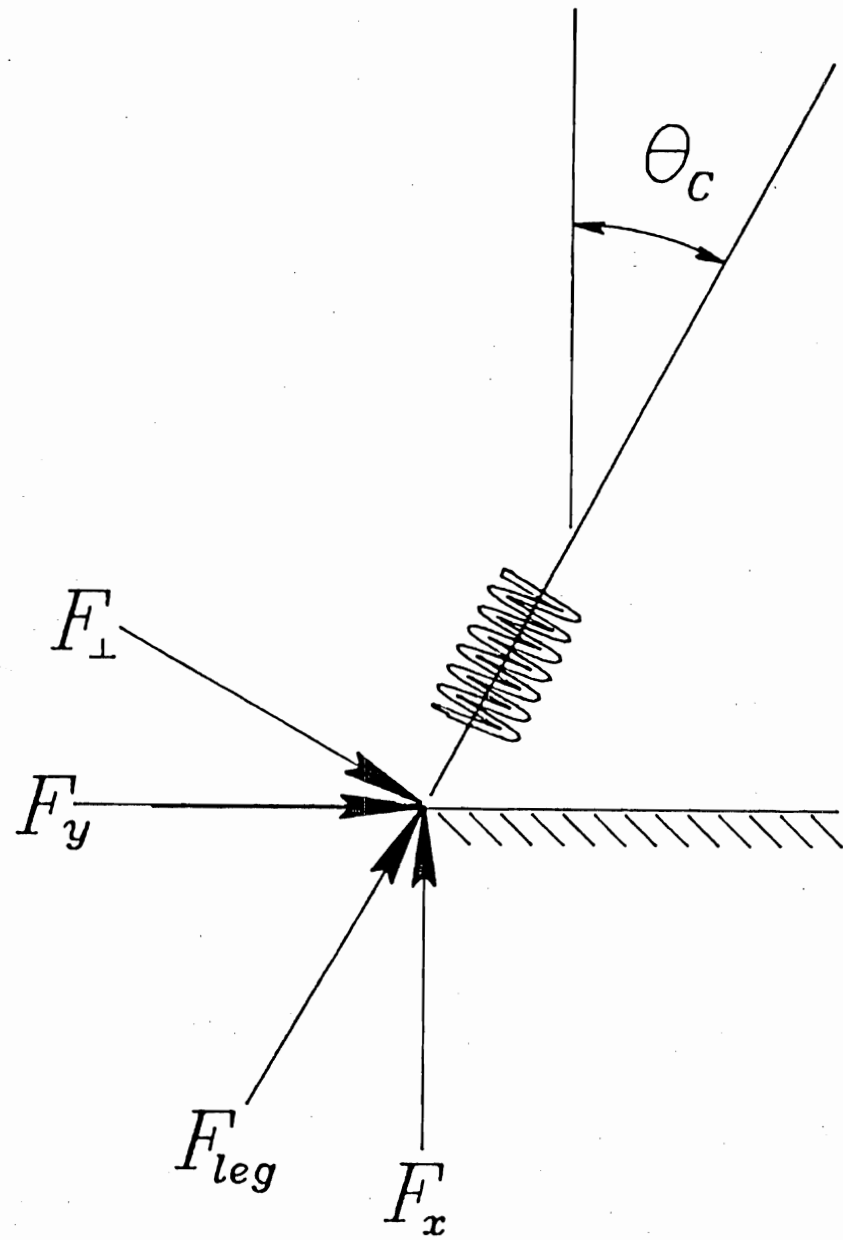


Figure 17 Notation for calculating contact forces using the finite-friction model.

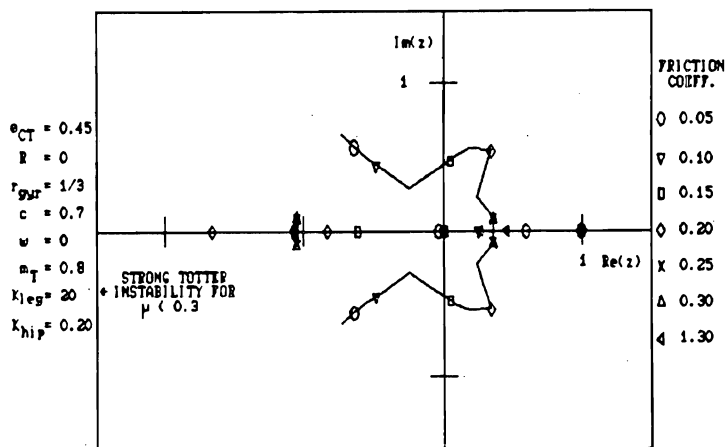
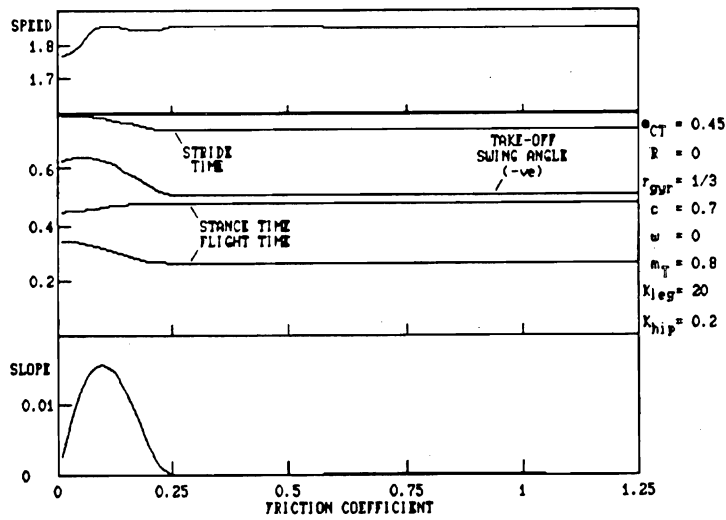


Figure 18a: This example shows features of the passive cycle for an otherwise conservative biped running on surfaces with various friction coefficients. Effects begin to appear on surfaces which a human runner would consider slippery (*i.e.* $\mu < 0.25$). Low friction leads to a complicated stance phase: it begins with the foot sliding forward very briefly; then backward for somewhat longer; then forward for an appreciable interval; then it remains at rest for awhile; and finally it takes off while sliding backward again.

Figure 18b: With finite friction the foot's slip rate can be specified as an independent initial condition for the running cycle. The number of initial conditions therefore totals 6, rather than 5 as in slip-free running. Thus the S-to-S equations have an additional "slip" mode. Its eigenvalue goes to zero in the high-friction limit, and remains quite close to $z = 0$ except on very slippery surfaces. As always, however, stability analysis focusses on the totter mode. This locus shows one totter eigenvalue splitting way down the negative real axis for surfaces with $\mu < 0.3$. Thus even though a steady cycle can be calculated for a slippery surface, as one might expect it would be hard to sustain.

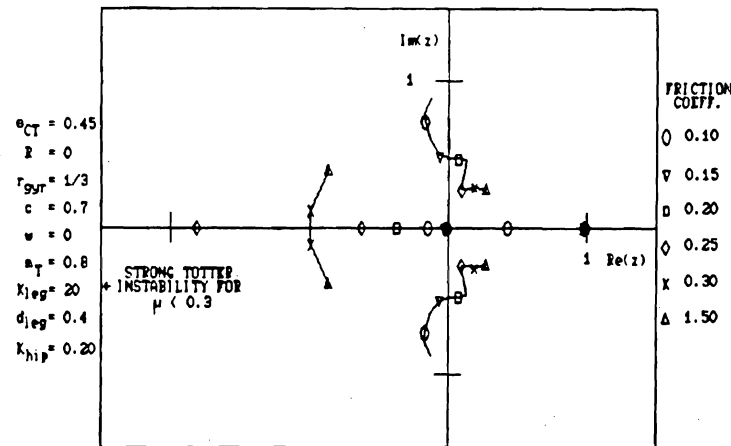
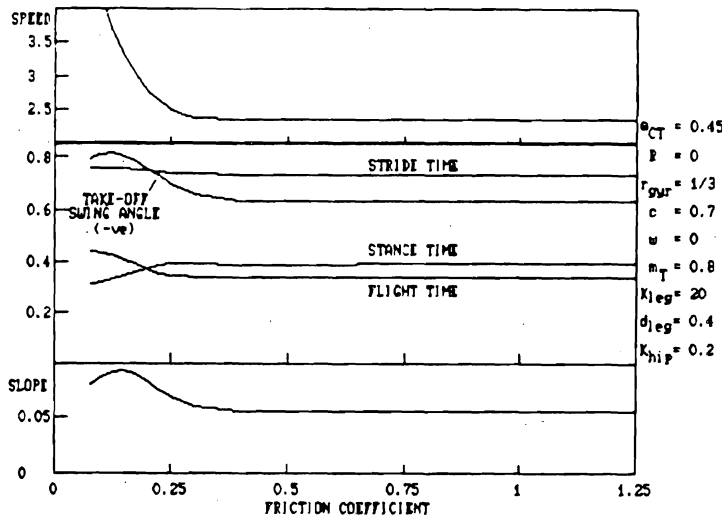


Figure 19a: This example shows the effect of friction on a biped which has stance damping, and therefore requires an appreciable slope to sustain the running cycle. The steady speed increases dramatically as the slope becomes slippery. One might well imagine the exhilaration of trying to run down an icy hill!

Figure 19b: Running down such a hill would be a very unstable proposition.

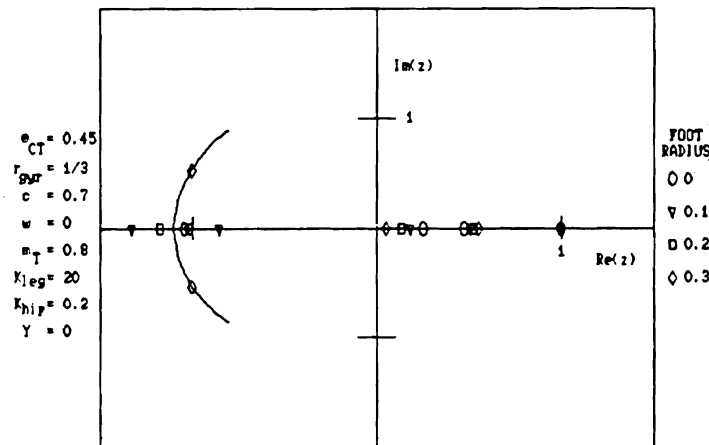
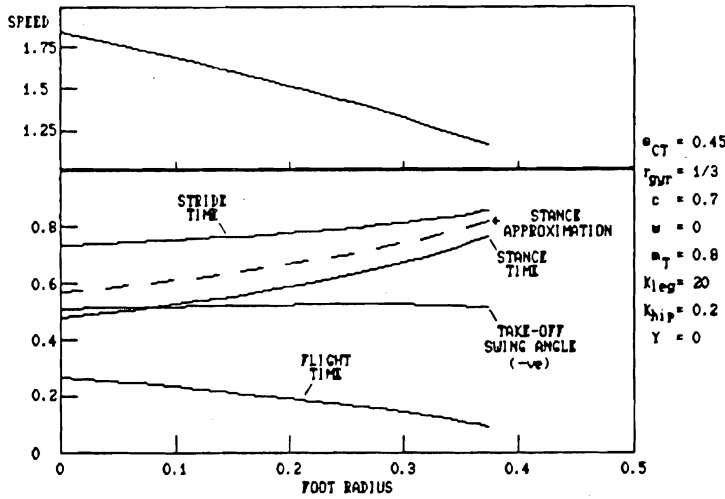


Figure 20a: Here the biped's foot radius is increased while all other parameters, including θ_{CT} , are held constant. The direct result is a reduction in centrifugal effect. An approximate 1D model of the stance rebound suggests a corresponding increase in stance time; this is verified by exact cycle calculations. Increasing stance time implies decreasing flight time and speed; at some point the flight phase becomes untenably short, and the cycle vanishes.

Figure 20b: A root locus *vs* foot radius shows destabilisation of the totter mode. (Note that the circular section is in fact the outer "totter arc".) This can be attributed to the decrease in speed (*cf.* figure 8). Speed and stability could be recovered by increasing θ_{CT} or K_{leg} .

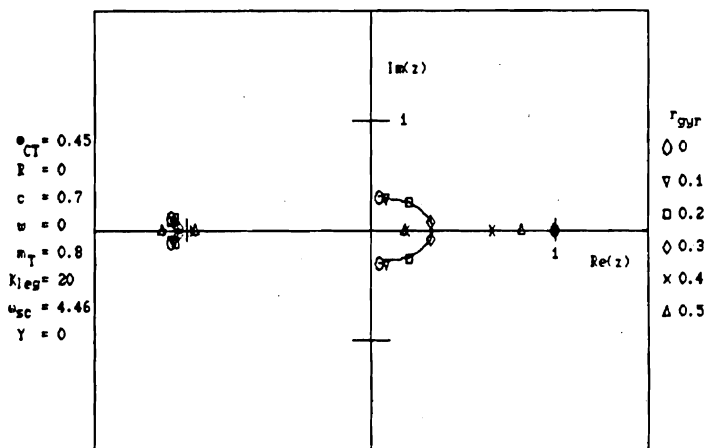
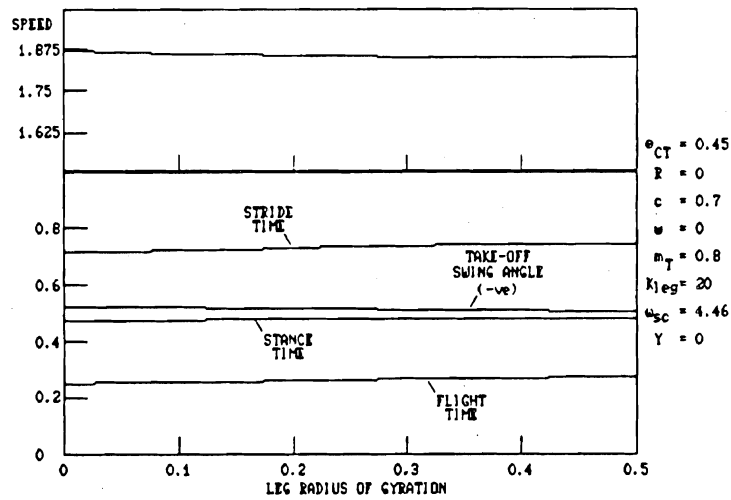


Figure 21a: A biped designer has a great deal of freedom in choosing the legs' moment of inertia, *provided* that he adjusts hip stiffness so that the scissor frequency remains constant. Here the inertia varies between the "point mass" and "dumbbell" limits, without significant effect on the running cycle.

Figure 21b: Changing inertia also has little direct effect on stability.

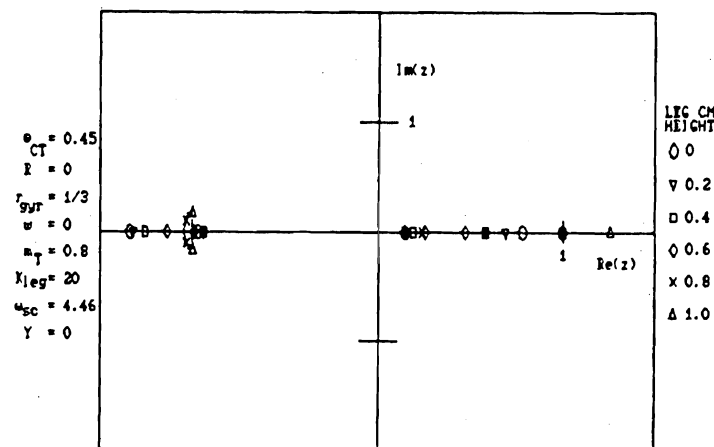
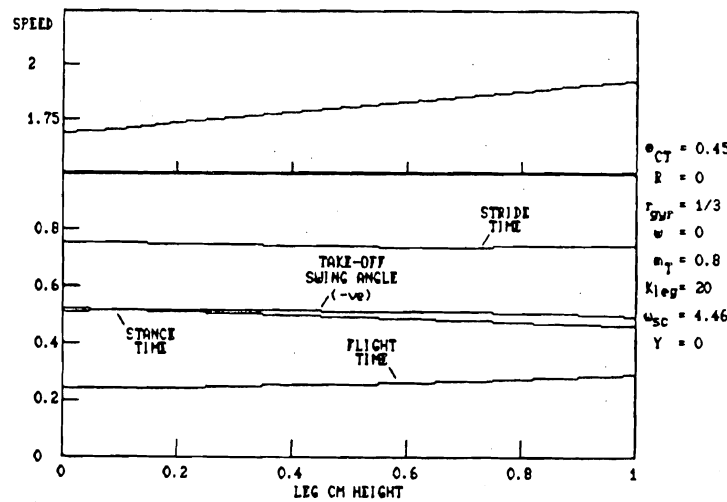


Figure 22a: In this example the scissor frequency is held constant while the legs' mass centre is shifted all the way from foot to hip. Only minor changes appear in the steady cycle; these are mediated by centrifugal effect. Thus provided that the legs are light (so that the biped's overall mass centre is nearly independent of c) the designer can put the leg's mass centre wherever is convenient.

Figure 22b: Changing c while keeping scissor frequency constant also has only minor effect on stability.

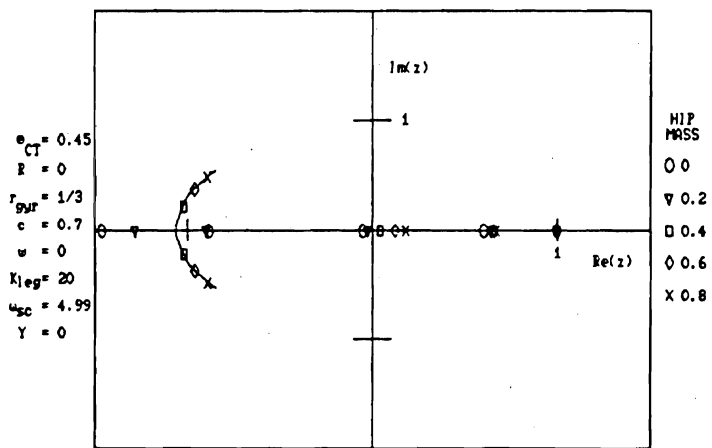
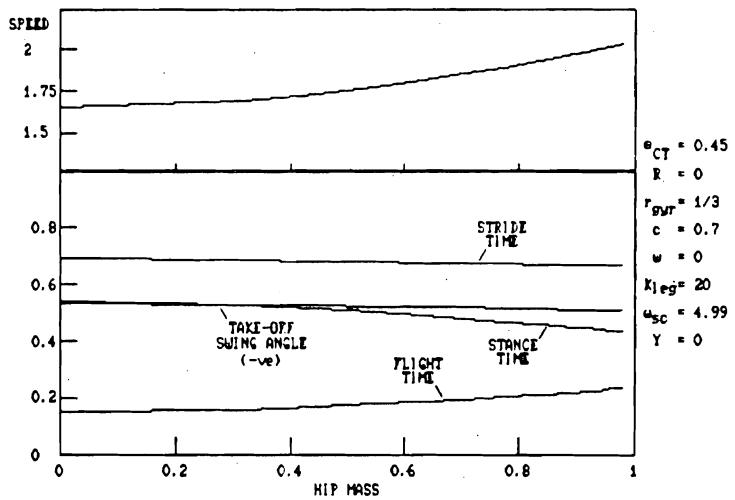


Figure 23a: Here mass is transferred from the legs to the torso. Hip stiffness is adjusted for constant scissor frequency. As in figure 22 the cycle is not sensitive to the mass distribution; again the small changes which appear are mediated by centrifugal effect during the stance rebound.

Figure 23b: Heavier legs are undesirable for stability, but the destabilising effects can be countered by increasing the cadence.